Article

Cell Reports

Tumor-Derived Lactic Acid Contributes to the Paucity of Intratumoral ILC2s

Graphical Abstract

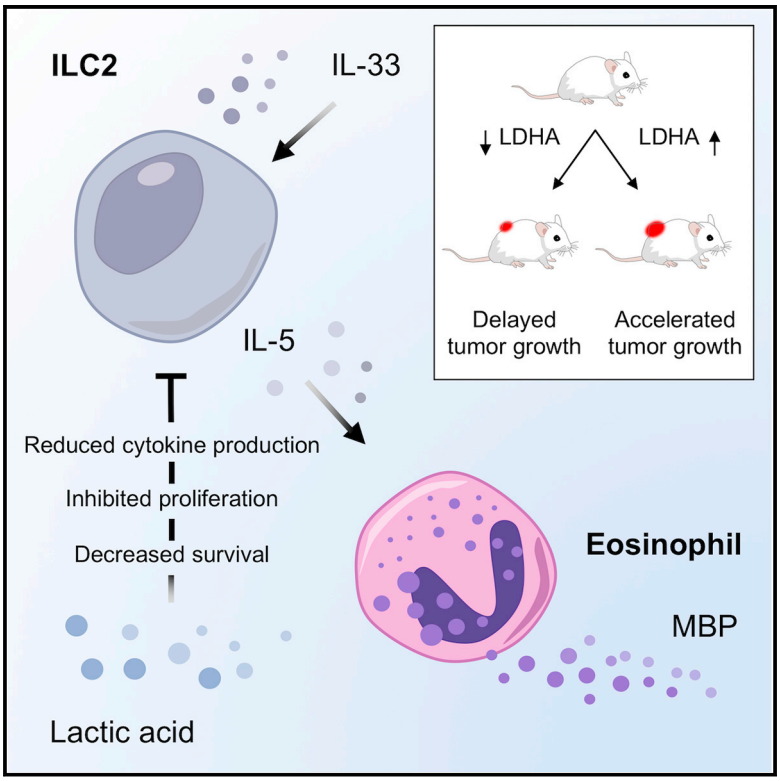

Highlights

- ILC2s are involved in eosinophil-associated antitumor responses in melanoma
- Lactic acid inhibits function and decreases survival of ILC2s
- Tumors with decreased lactic acid production exhibit increased infiltration of ILC2s

Authors

Marek Wagner, Kafi N. Ealey, Hiroe Tetsu, Tsuyoshi Kiniwa, Yasutaka Motomura, Kazuyo Moro, Shigeo Koyasu

Correspondence

marek.wagner@uib.no (M.W.), shigeo.koyasu@riken.jp (S.K.)

In Brief

Wagner et al. demonstrate, using melanoma as a model, that group 2 innate lymphoid cells (ILC2s) activated by IL-33 potentiate the eosinophil-associated antitumor response. In contrast, lactate production by melanoma cells impairs function and survival of ILC2s, leading to an enhanced tumor growth.

Wagner et al., 2020, Cell Reports *30*, 2743–2757
February 25, 2020
https://doi.org/10.1016/j.celrep.2020.01.103

CellPress

Cell Reports
Article

Tumor-Derived Lactic Acid Contributes to the Paucity of Intratumoral ILC2s

Marek Wagner,[1,2,3,*] Kafi N. Ealey,[2] Hiroe Tetsu,[2,4] Tsuyoshi Kiniwa,[2] Yasutaka Motomura,[2,5] Kazuyo Moro,[2,4,5,6] and Shigeo Koyasu[1,7,8,*]

[1]Laboratory for Immune Cell Systems, RIKEN Center for Integrative Medical Sciences, Yokohama, Japan
[2]Laboratory for Innate Immune Systems, RIKEN Center for Integrative Medical Sciences, Yokohama, Japan
[3]Department of Biomedicine, University of Bergen, Bergen, Norway
[4]Department of Medical Life Science, Graduate School of Medical Life Science, Yokohama City University, Yokohama, Japan
[5]Laboratory for Innate Immune Systems, Department of Microbiology and Immunology, Osaka University Graduate School of Medicine, Osaka, Japan
[6]Laboratory for Innate Immune Systems, Immunology Frontier Research Center (IFReC), Osaka University Graduate School of Medicine, Osaka, Japan
[7]Department of Microbiology and Immunology, Keio University School of Medicine, Tokyo, Japan
[8]Lead Contact
*Correspondence: marek.wagner@uib.no (M.W.), shigeo.koyasu@riken.jp (S.K.)
https://doi.org/10.1016/j.celrep.2020.01.103

SUMMARY

Group 2 innate lymphoid cells (ILC2s) are abundant in non-lymphoid tissues and increase following infectious and inflammatory insults. In solid tumors, however, ILC2s constitute a relatively small proportion of immune cells. Here, we show, using melanoma as a model, that while the IL-33/IL C2/eosinophil axis suppresses tumor growth, tumor-derived lactate attenuates the function and survival of ILC2s. Melanomas with reduced lactate production (LDHA^{low}) are growth delayed and typified by an increased number of ILC2s compared with control tumors. Upon IL-33 stimulation, ILC2s accompanied by eosinophils more effectively restrain the growth of LDHA^{low} tumors than control melanomas. Furthermore, database analysis reveals a negative correlation between the expression of *LDHA* and markers associated with ILC2s and the association of high expression of *IL33* and an eosinophil marker *SIGLEC8* with better overall survival in human cutaneous melanoma patients. This work demonstrates that the balance between the IL-33/ILC2/eosinophil axis and lactate production by tumor cells regulates melanoma growth.

INTRODUCTION

Innate lymphoid cells (ILCs) are lymphocytes that mirror the phenotypes and functions of T cells. However, ILCs lack somatically rearranged antigen receptors and cell-surface molecules that identify their immune cell ancestry (Artis and Spits, 2015). Based on the signature cytokines produced and the developmental trajectories acquired, ILCs have been classified into five subsets: natural killer (NK) cells, group 1 innate lymphoid cells (ILC1s), ILC2s, ILC3s and lymphoid tissue inducer (LTi) cells (Spits et al., 2013; Artis and Spits, 2015; Vivier et al., 2018).

ILC2s depend on GATA3 and RORα for their development (Spits et al., 2013; Mjosberg et al., 2012; Furusawa et al., 2013). While described as lineage marker-negative (Lin$^-$) cells, ILC2s express various cell surface markers such as c-Kit (CD117), Sca1 (Ly6a), KLRG1, ICOS, and IL-7Rα (CD127) (Mattner and Wirtz, 2017; Moro et al., 2010, 2016). ILC2s respond to the alarmin cytokines interleukin (IL)-33, IL-25, and thymic stromal lymphopoietin (TSLP, combined with IL-33) in addition to eicosanoids such as prostaglandin D2 and leukotriene D4, neuropeptides including neuromedin U, and sex hormones (Kabata et al., 2018). Following activation, they rapidly expand and produce cytokines such as IL-4, IL-5, IL-9, IL-13, and/or amphiregulin (Moro et al., 2010; Neill et al., 2010; Price et al., 2010; Kabata et al., 2013).

ILC2s are rare in secondary lymphoid organs relative to other immune cells (Vivier et al., 2016). Instead, they harbor a unique location within non-lymphoid tissues, especially skin and mucosal barriers (i.e., respiratory and intestinal mucosa), and in fat-associated lymphoid clusters (FALCs) in the visceral adipose tissue (Moro et al., 2010; Hammad and Lambrecht, 2015; Mohapatra et al., 2016; Von Moltke et al., 2016). ILC2s provide the first line of defense against helminths and protect the integrity of the epithelium (Artis and Spits, 2015). They are also implicated in the regulation of metabolic homeostasis (Brestoff et al., 2015; Sasaki et al., 2019). Notably, dysregulation of ILC2s has been associated with the development of autoimmune and inflammatory diseases (Cephus et al., 2017; Ealey et al., 2017; Ebbo et al., 2017).

Whereas the importance of NK cells in the antitumor response is firmly rooted, the role of ILC2s remains ambiguous and poorly understood, partially due to their low abundance in solid tumors (Mattner and Wirtz, 2017; Wagner et al., 2017; Carrega et al., 2015). The acquisition of antitumorigenic functions appears to depend on the context of tumor specificity and signaling intensity (Wagner et al., 2017). Recent evidence indicates that metabolic pathways within the tumor microenvironment shape the diversity of infiltrating immune cells (Biswas, 2015; Chang et al., 2015; Colegio et al., 2014; Brand et al., 2016; Lyssiotis and Kimmelman, 2017). However, the extent to which metabolic

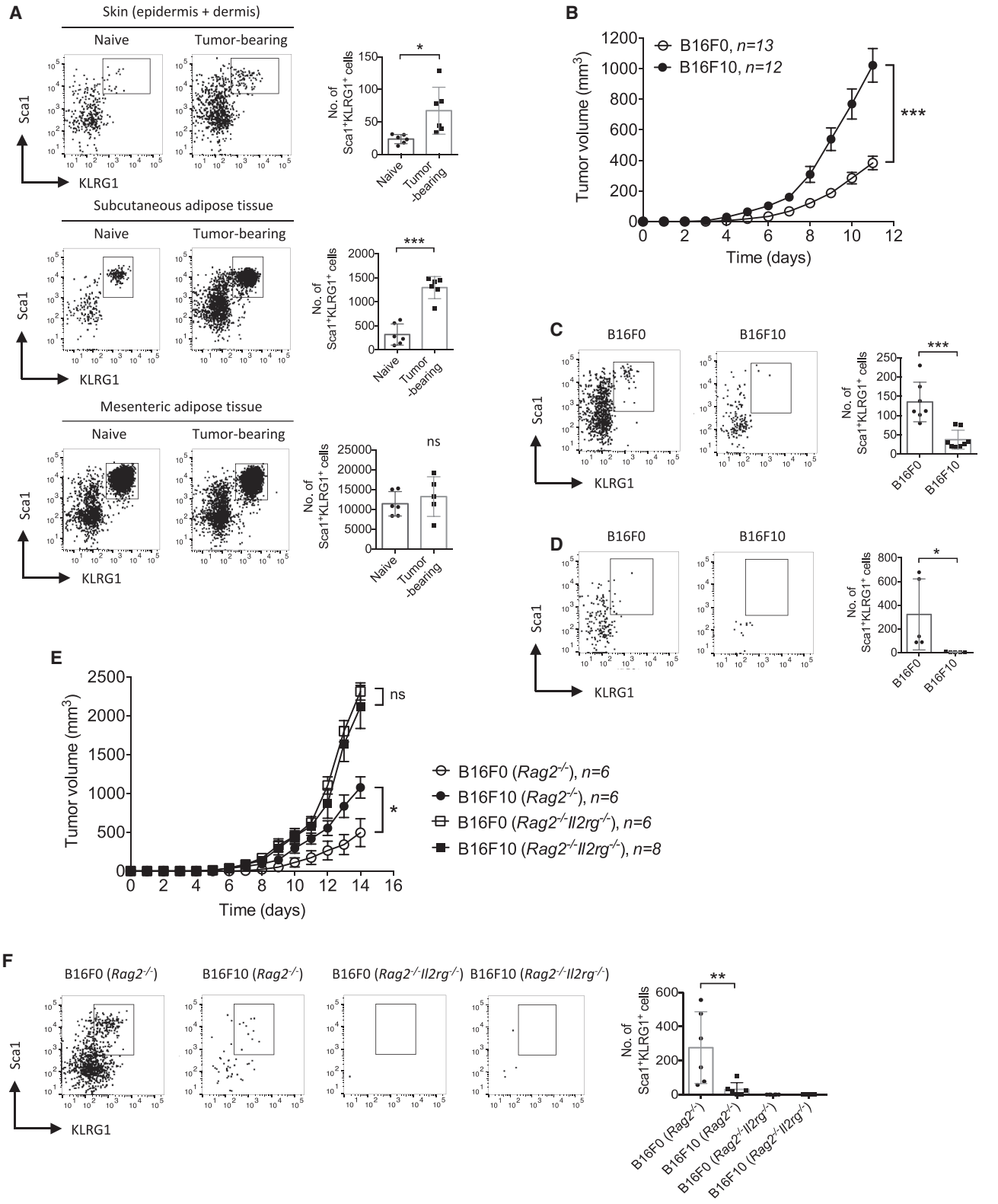

Figure 1. Rapidly Growing B16F10 Tumors Are Depleted of ILC2s

(A) Representative plots and analysis of ILC2 populations in the skin (n = 6) and subcutaneous (n = 6) and mesenteric adipose tissue (n = 6) from naive and tumor-bearing mice by flow cytometry.

(legend continued on next page)

deviations from normal set points affect intratumoral ILC2s has not yet been assessed.

Glucose uptake and metabolism is accelerated in tumor cells by an increased expression of glucose transporters and glycolytic enzymes such as glucose transporter 1 (GLUT1) and lactate dehydrogenase A (LDHA), respectively (Vander Heiden et al., 2009; Gatenby and Gillies, 2004; Hay, 2016). In addition, the continuous export of lactate and protons (lactic acid [LA]) by means of monocarboxylate transporters (MCTs) drives the glycolytic metabolism forward to adapt to the anabolic demands of tumor cells (Doherty and Cleveland, 2013). This process leads to the accumulation of LA and subsequent acidification of the tumor microenvironment (Doherty and Cleveland, 2013; Vander Heiden et al., 2009; Gatenby and Gillies, 2004; Hay, 2016). Increased lactate production has been associated with the enhanced progression of various tumor types, including melanoma (Girgis et al., 2014; Walenta et al., 2000; Petrelli et al., 2015; Hirschhaeuser et al., 2011).

Here, using melanoma as a model, we unravel an immunosuppressive activity imposed on ILC2s by tumor cells through the accumulation of LA in the tumor microenvironment. We show that LA inhibited proliferation and cytokine production, and subsequently decreased the survival of ILC2s *in vitro*. Interference with this immunosuppressive axis in B16F10 melanomas by specifically knocking down lactate dehydrogenase A ($LDHA^{low}$) significantly increased the number of intratumoral ILC2s. Following stimulation with IL-33, the expansion of ILC2s within $LDHA^{low}$ B16F10 tumors accompanied by eosinophils more effectively controlled melanoma growth compared with control tumors. It is worth noting that an analysis of the gene expression data of human cutaneous melanomas revealed that the expression of *LDHA* negatively correlated with markers associated with ILC2s. Moreover, the high expression of *IL33* and an eosinophil marker *SIGLEC8* was associated with better overall survival in cutaneous melanoma patients, indicating the role of the IL-33/ILC2/eosinophil axis in anti-melanoma immunity.

Our results identify tumor-derived LA production as a plausible immunosuppressive mechanism that contributes to the paucity of intratumoral ILC2s.

RESULTS

Exclusion of Intratumoral ILC2s in B16 Tumors

Given that ILC2s are numerous in certain tissues, we assessed the number of ILC2s in the skin and subcutaneous and mesenteric adipose tissues in naive and tumor-bearing mice using B16 melanomas as a model. We subcutaneously inoculated wild-type (WT) C57BL/6 mice with highly malignant B16F10 melanoma cells (1×10^6 cells per mouse). On day 11 post-inoculation, the skin overlying the tumor mass and neighboring subcutaneous adipose tissue, together with mesenteric adipose tissue, were carefully collected and analyzed for the presence of ILC2s using flow cytometry. After gating on live and Lin^-CD45^+ cells, the analysis revealed a roughly 3- and 4-fold increase in the number of $Sca1^+KLRG1^+$ ILC2s in the skin and subcutaneous adipose tissue from tumor-bearing mice compared with homeostatic cutaneous and subcutaneous ILC2 populations, respectively (Figures 1A, upper and center panels, and S1). In contrast, there was no significant difference in the number of $Sca1^+KLRG1^+$ ILC2s in the mesenteric adipose tissue between naive and tumor-bearing mice (Figure 1A, lower panel). Spurred by the observation that the tissues adjacent to the tumor mass were replete with ILC2s, we next assessed the number of intratumoral ILC2s. For that reason, we subcutaneously inoculated WT C57BL/6 mice with either weakly (B16F0) or highly metastatic (B16F10) melanoma cells (1×10^6 cells per mouse). As expected, B16F10 melanomas grew more rapidly and reached ~1 cm^3 (±0.1 cm^3, SEM) in size, whereas their less-malignant counterparts, B16F0 melanomas, reached ~0.4 cm^3 (±0.04 cm^3, SEM) in size within 11 days post-inoculation (Figure 1B). Tumors were then collected and analyzed for the presence of intratumoral ILC2s. While flow cytometric analysis showed a relatively low abundance of $Sca1^+KLRG1^+$ ILC2s in both tumor types, a significantly lower number of ILC2s was observed in B16F10 melanomas compared with B16F0 tumors (Figure 1C). Moreover, $Sca1^+KLRG1^+$ ILC2s were entirely or almost completely depleted in B16F10 melanomas following sacrifice at a later time point, on day 14 post-inoculation (Figure 1D).

To exclude the possibility that architectural changes within the skin surrounding the tumors could influence immune cell infiltration (Gajewski et al., 2013), we performed a histological analysis of paraffin-embedded tumor sections. As judged by Picrosirius Red staining, we found no apparent difference in collagen density (Figure S2A) within the skin surrounding B16F0 and B16F10 tumors. However, we did find a decreased number of dermal adipocytes in the skin surrounding B16F10 tumors, as revealed by immunohistochemical analysis using an antibody against the lipid droplet-associated protein Perilipin1 (Figures S2B and S2C). To further characterize tumor-associated adipose tissue, we implanted B16F10 melanoma cells into one of the anterior subcutaneous adipose tissue depots in WT C57BL/6 mice, as previously described (Wagner et al., 2012). Immunohistochemical analysis on day 14 post-inoculation revealed the abundance of IL-33 within subcutaneous adipose tissue from tumor-bearing mice, as particularly exemplified by the

(B) Tumor growth profiles of B16F0 and B16F10 cells (1×10^6 cells per mouse) subcutaneously injected into C57BL/6 mice (n = 12–13).
(C) Representative flow cytometry plots and quantification of ILC2 populations in the tumors (n = 7–8) on day 11 post-inoculation.
(D) Representative flow cytometry plots and quantification of ILC2 populations in the tumors (n = 5) on day 14 post-inoculation.
(E) Tumor growth profiles after subcutaneous injection of B16F0 and B16F10 cells (1×10^6 cells per mouse) into immunodeficient $Rag2^{-/-}$ and $Rag2^{-/-}Il2rg^{-/-}$ mice (n = 6–8).
(F) Representative flow cytometry plots and quantification of tumor-infiltrating ILC2 populations (n = 6).
All of the results from tumor growth studies were combined from two independent experiments. The flow cytometry results shown are from one representative experiment out of two independent experiments. The "n" indicates the number of biological replicates. $p < 0.05$ considered significant; *$p < 0.05$; **$p < 0.01$; ***$p < 0.001$ as determined by Student's t test or one-way ANOVA, followed by Tukey's multiple comparisons test. Error bars represent SEMs.

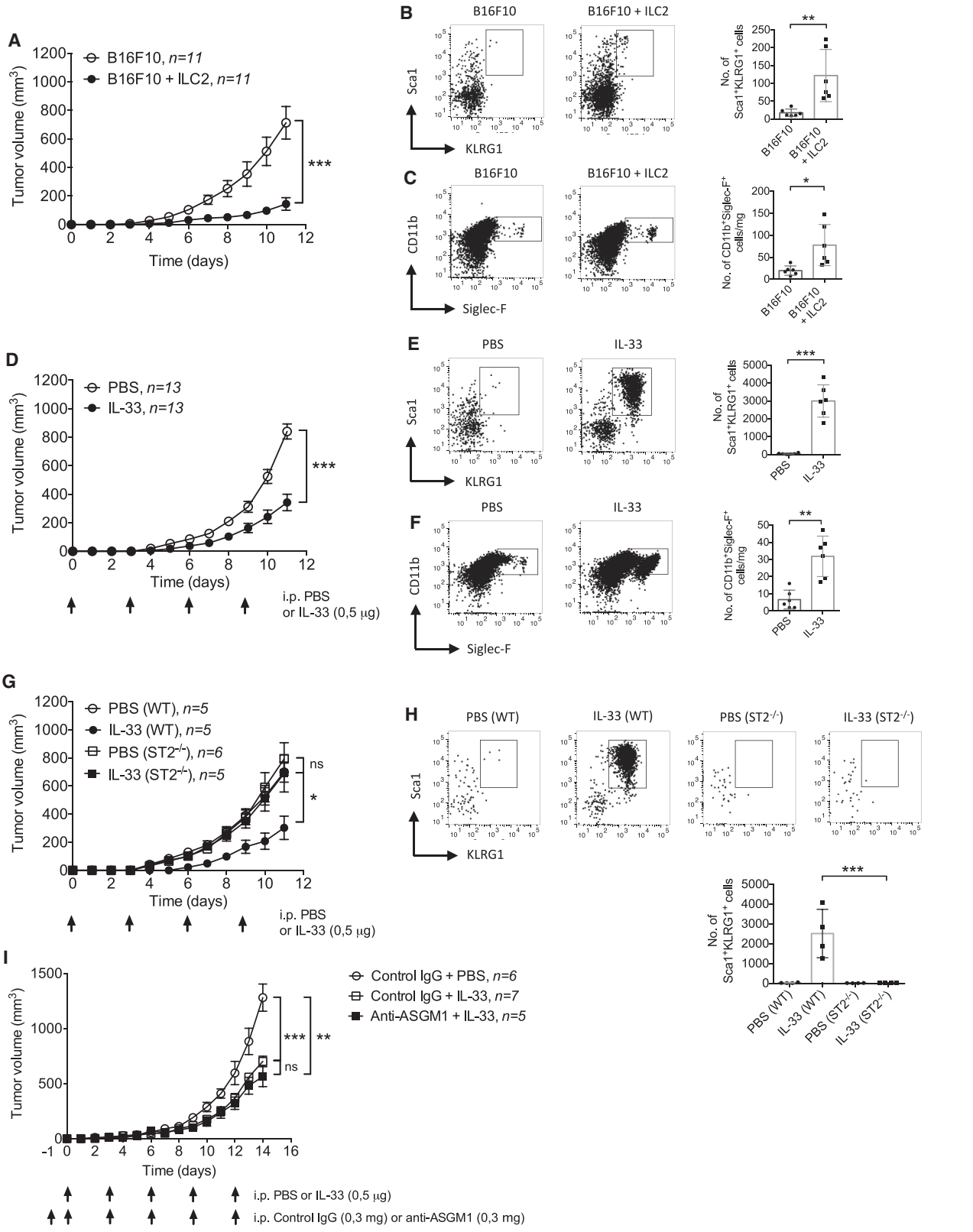

(legend on next page)

presence of infiltrating inflammatory cells positively stained for IL-33 (Figure S2D).

Mirroring the decrease in the number of ILC2s, we found a reduced number of intratumoral T cells ($CD3^+$ and $CD8^+$ cells) and myeloid lineage cells ($CD11b^+$ cells) in B16F10 tumors compared with their less malignant counterparts, B16F0 tumors, with the exception of macrophages ($F4/80^+$ cells), as their number remained unchanged (Figures S3A and S3B). Since changes in vascular endothelium may influence the growth and contribute to the observed phenotype of B16F10 tumors, we assessed blood and lymphatic vessel densities (Lund et al., 2016; Steinskog et al., 2016). Although blood vessel density was reduced in B16F10 tumors compared with their less malignant counterparts, as analyzed by the number of $CD31^+$ structures per field of view, the percentage of area covered by $CD31^+$ structures was noticeably increased in B16F10 tumors (Figures S3C and S3D). There was no significant difference in lymphatic vessel densities, as revealed by the number of $Lyve1^+$ structures (Figure S3E).

To investigate whether the low abundance of immune cells within B16F10 tumors could provide a selective growth advantage over their less malignant counterparts, we inoculated immunodeficient *Rag2*$^{-/-}$ mice (lacking mature B, T, and NKT cells) and *Rag2*$^{-/-}$*Il2rg*$^{-/-}$ mice (lacking ILCs, apart from mature B, T, and NKT cells) with B16 melanoma cells. In contrast to that in *Rag2*$^{-/-}$ mice, the growth difference between B16F0 and B16F10 melanomas was lost in *Rag2*$^{-/-}$*Il2rg*$^{-/-}$ mice (Figure 1E). Furthermore, flow cytometric analysis confirmed the absence of ILC2s within both B16F0 and B16F10 tumors in *Rag2*$^{-/-}$*Il2rg*$^{-/-}$ mice (Figure 1F). As observed with WT mice, a significantly lower number of ILC2s was found in B16F10 melanomas compared with B16F0 tumors in *Rag2*$^{-/-}$ mice (Figure 1F).

Overall, it is likely that these results rule out the possibility that the low abundance of ILC2s in B16F10 tumors is due to their decreased ability to penetrate the tumor tissue. Instead, our data suggest that the tumor microenvironment negatively affects ILC2s to suppress their potential antitumor activity.

IL-33 Controls B16F10 Tumor Growth and Intratumoral Expansion of ILC2s

To reveal the potential antitumorigenic properties of ILC2s, we subcutaneously inoculated WT C57BL/6 mice with B16F10 melanoma cells alone (1×10^6 cells per mouse) or together with ILC2s (1×10^5 cells per mouse). The presence of ILC2s controlled the growth of B16F10 tumors (Figure 2A), although the number of intratumoral ILC2s was strikingly decreased on day 11 post-inoculation. The median number of cells was 91 (n = 6) for $Sca1^+KLRG1^+$ ILC2s (Figure 2B). A significant increase in the number of $CD11b^+Siglec\text{-}F^+$ eosinophils was observed in tumors growing with ILC2s compared with tumors growing alone (Figure 2C).

To experimentally probe the role of IL-33 in the generation of ILC2-mediated response against B16F10 tumors, we subcutaneously inoculated WT C57BL/6 mice with tumor cells (1×10^6 cells per mouse) and intraperitoneally administered IL-33 (0.5 μg in 100 μL PBS) or PBS at the time of inoculation and every 3 days thereafter. The administration of IL-33 significantly suppressed the growth of B16F10 melanomas (Figure 2D). In addition, flow cytometric analysis revealed a striking increase in the number of $Sca1^+KLRG1^+$ ILC2s (Figure 2E) and $CD11b^+$ $Siglec\text{-}F^+$ eosinophils (Figure 2F) in B16F10 tumors from IL-33-treated mice. To determine whether the antitumor activity of IL-33 is mediated directly or indirectly through binding to its receptor, we subcutaneously inoculated *Il1rl1*$^{-/-}$ mice (referred to as ST2$^{-/-}$ mice) lacking the functional IL-33 receptor with B16F10 cells (1×10^6 cells per mouse). In contrast to WT mice, the difference in tumor growth between mice treated with IL-33 or PBS was lost in ST2$^{-/-}$ mice (Figure 2G). Although flow cytometric analysis confirmed the increase in the number of $Sca1^+KLRG1^+$ ILC2s in B16F10 tumors from IL-33-treated WT mice, no difference was observed in tumors implanted into ST2$^{-/-}$ mice, regardless of the type of treatment chosen (Figure 2H). To exclude the possibility that IL-33 directly activates T cells or NK cells to mediate the observed antitumor response, we depleted Rag2$^{-/-}$ mice of NK cells using anti-asialo GM1 (ASGM1) antibody during IL-33 treatment. We found no difference in the tumor growth between Rag2$^{-/-}$ mice depleted of NK cells and Rag2$^{-/-}$ mice that received control immunoglobulin G (IgG) during IL-33 treatment (Figure 2I). Nevertheless, tumors in both groups of mice that received IL-33 treatment grew significantly slower compared with the group of mice treated with PBS only (Figure 2I).

In addition, histological analysis of tumor sections revealed the presence of lymphoid clusters surrounding tumors from

Figure 2. B16F10 Tumors Challenged with IL-33 Are Growth Delayed and Enriched with ILC2s and Eosinophils

(A) Tumor growth profiles of B16F10 cells (1×10^6 cells per mouse) subcutaneously injected alone or admixed with ILC2s (1×10^5 cells per mouse) (n = 11).

(B and C) Representative flow cytometry plots and quantification of tumor-infiltrating (B) ILC2s and (C) eosinophils (n = 6).

(D) Tumor growth profiles after subcutaneous injection of B16F10 cells (1×10^6 cells per mouse) into PBS or IL-33-treated C57BL/6 mice (n = 13). The mice were subjected to treatment with IL-33 (0.5 μg in 100 μL PBS) or PBS at the time of tumor cell injection and every 3 days thereafter (as indicated by arrows).

(E and F) Representative flow cytometry plots and quantification of tumor-infiltrating (E) ILC2s and (F) eosinophils. (n = 6).

(G) Tumor growth profiles of B16F10 cells (1×10^6 cells per mouse) subcutaneously injected either into *Il1rl1*$^{-/-}$ mice (referred to as ST2$^{-/-}$ mice), which lack the receptor for IL-33 or wild-type (WT) mice (n = 5–6 mice per group). The mice were subjected to the treatment with IL-33 (0.5 μg in 100 μL PBS) or PBS at the time of tumor cell injection and every 3 days thereafter (as indicated by the arrows).

(H) Representative flow cytometry plots and quantification of tumor-infiltrating ILC2s (n = 4).

(I) Growth of B16F10 cells (1×10^6 cells per mouse) subcutaneously inoculated into Rag2$^{-/-}$ mice (n = 5–7) depleted of NK cells during IL-33 treatment. The mice were injected either with anti-asialo GM1 (ASGM1) antibody (0.3 mg in 100 μL PBS) or control IgG (0.3 mg in 100 μL PBS) and subjected either to the treatment with IL-33 (0.5 μg in 100 μL PBS) or PBS as indicated by the arrows.

All of the results from tumor growth studies were combined from two independent experiments. The flow cytometry results shown are from one representative experiment out of two independent experiments. The "n" indicates the number of biological replicates. $p < 0.05$ considered significant; *$p < 0.05$; **$p < 0.01$; ***$p < 0.001$ as determined by Student's t test or one-way ANOVA followed by Tukey's multiple comparisons test. Error bars represent SEMs.

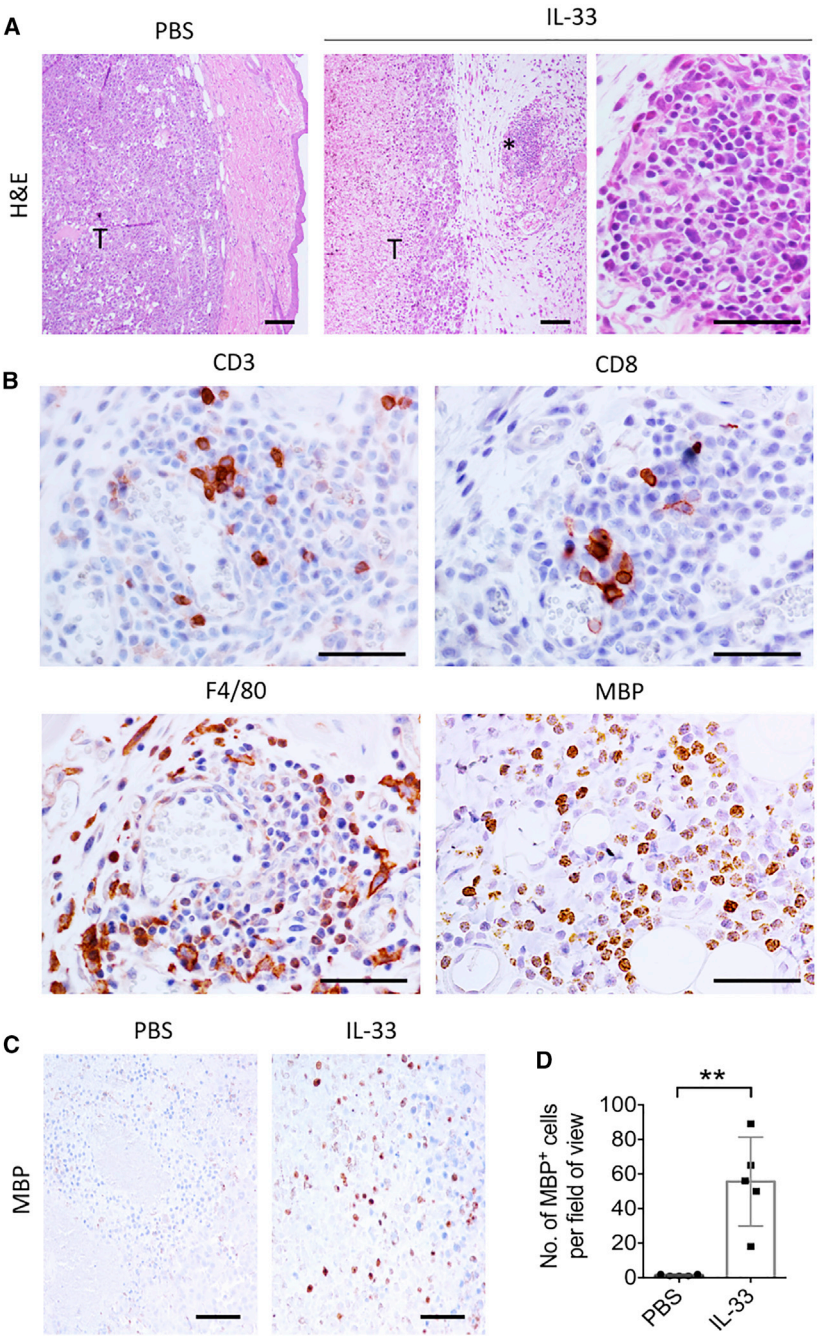

Figure 3. IL-33-Activated ILC2s Integrate within Lymphoid Clusters Formed Around B16F10 Tumors

(A) Histological analysis of hematoxylin and eosin (H&E)-stained sections of B16F10 tumors harvested at day 11 post-inoculation from PBS or IL-33-treated mice. "T" indicates tumor. "*" indicates a lymphoid cluster, which is enlarged in the right panel.

(B) Immunohistochemical analysis of immune infiltrates integrated within lymphoid clusters formed around tumors from IL-33-treated mice.

(C and D) Immunohistochemical analysis (C) and quantification (D) of MBP$^+$ cells present in the periphery and throughout the interior of the tumors from PBS- or IL-33-treated mice (n = 5).

The "n" indicates the number of biological replicates. $p < 0.05$ considered significant; ***$p < 0.01$ as determined by Student's t test. The error bars represent SEMs. The average number of cells from 5 fields of view per tumor in (D). Scale bars: H&E 100 μm (short) and 50 μm (long); immunohistochemistry (IHC) 100 μm.

IL-33-treated WT C57BL/6 mice only, as judged by hematoxylin and eosin (H&E) staining (Figure 3A). Immunohistochemical analysis revealed the presence of T cells and eosinophils within clusters and macrophages scattered around (Figure 3B). We found the number of eosinophils expressing major basic protein (MBP) in the periphery as well as throughout the interior of the tumors from IL-33-treated mice strikingly increased compared with PBS-treated mice (Figures 3C and 3D). No statistically significant difference in the number of CD3$^+$ or CD8$^+$ cells, however, was observed in B16F10 tumors from IL-33-treated mice compared with controls following immunohistochemical (Figures S4A and S4B) and flow cytometric analyses (data not shown). Instead, we found an increased number of macrophages typified as alternatively activated by expression of the macrophage galactose C-type lectin 10A (CLEC10A/CD301) in tumor samples from IL-33-treated mice. The majority of CD301$^+$ macrophages, but not F4/80$^+$ macrophages, were found in the skin surrounding the tumors (Figures S4C and S4D). A similar staining pattern was observed using another marker for alternatively activated macrophages, CD163 (data not shown).

These results support the notion of an anti-tumorigenic role of ILC2/eosinophil axis in melanoma, which can be further enhanced following IL-33 stimulation.

Tumor Cell-Derived LA has an Inhibitory Effect on ILC2s

To study interactions between tumor cells and ILC2s using an *in vitro* model that replicates many features of solid tumors *in vivo*, we generated spheroids from B16F0 and B16F10 melanoma cells and co-cultured them with ILC2s. Within 5 days of incubation, we noticed a significant shift in pH, as indicated by a change in the color of medium from red to light yellow in co-cultures of spheroids with ILC2s (data not shown). More importantly, the presence of spheroids selectively decreased the number of ILC2s co-cultured in medium supplemented with IL-2 plus IL-33 but not IL-2 alone (Figure 4A). We assumed that tumor cell-derived signals inhibited the proliferation of IL-33-stimulated ILC2s. To test this possibility, we collected conditioned medium (CM) supplemented with IL-2 plus IL-33 from B16F10 cells. CM was sufficient

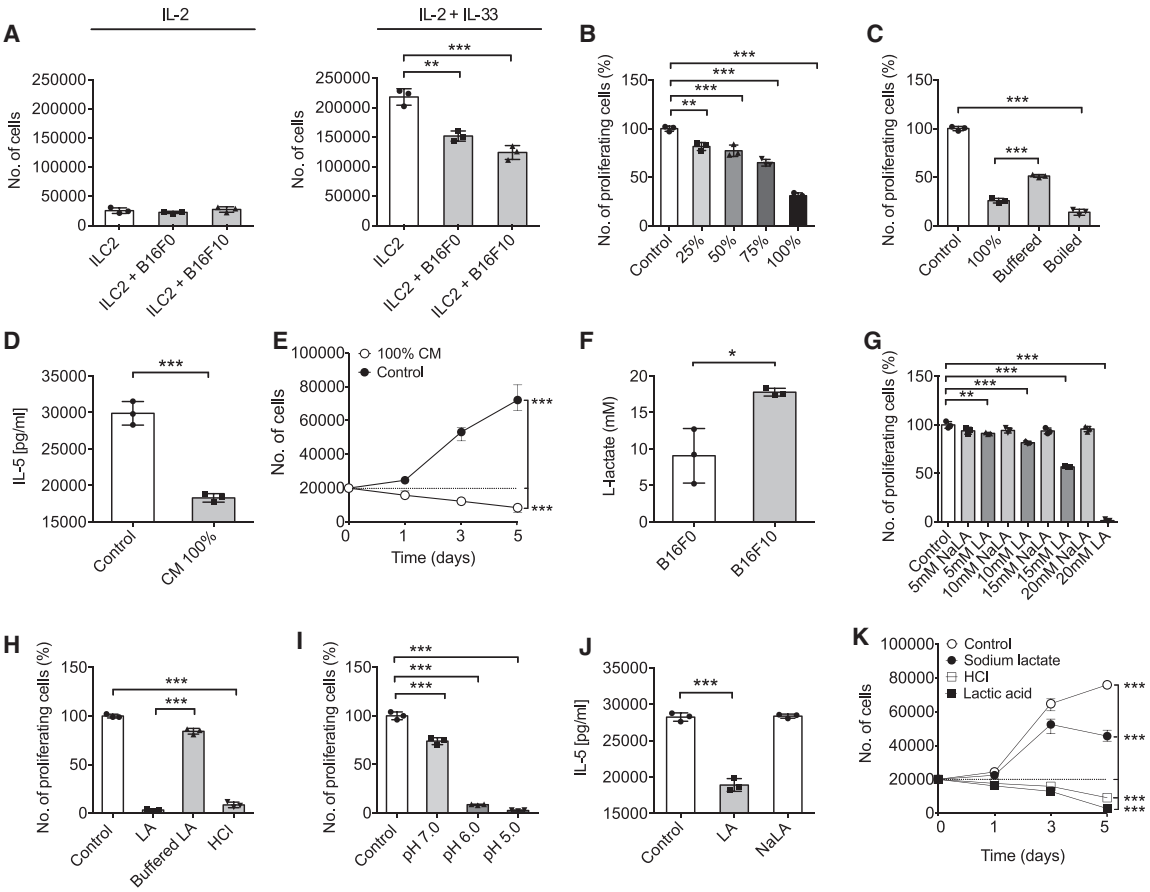

Figure 4. Lactic Acid (LA) Impairs *In Vitro* Proliferation, IL-5 Production, and Survival of ILC2s

(A) Quantification of the number of ILC2s co-cultured with B16F0 or B16F10 spheroids in medium supplemented with IL-2 (left) or IL-2 plus IL-33 (right) for a period of 5 days (n = 3).

(B and C) Assessment of the proliferative potential of ILC2s incubated either in different concentrations of conditioned medium (CM) from B16F10 cells supplemented with IL-2 plus IL-33 (B) and its buffered (pH 7.4) or boiled (100°C) derivatives for 24 h (n = 3) (C).

(D) Analysis of IL-5 levels produced by ILC2s cultured for 24 h in CM (n = 3).

(E) Quantification of the number of ILC2s after culture in CM for a period of 5 days (n = 3).

(F) Analysis of the level of LA present in medium from B16F0 and B16F10 spheroids co-cultured with ILC2s in medium supplemented with IL-2 plus IL-33 for a period of 3 days (n = 3).

(G) Assessment of the proliferative potential of ILC2s incubated in different concentrations of LA and sodium lactate (NaLA) supplemented with IL-2 plus IL-33.

(H and I) Assessment of the proliferative potential of ILC2s incubated in buffered (H, pH 7.4) and acidified (I) medium with varying concentrations of HCl supplemented with IL-2 plus IL-33 (n = 3).

(J) Analysis of IL-5 levels produced by ILC2s cultured for 24 h in 20 mM LA or 20 mM NaLA (n = 3).

(K) Quantification of the number of ILC2s after culture in medium containing 20 mM LA, 20 mM NaLA, or HCl (pH = 6.0) for a period of 5 days (n = 3).

Unless otherwise stated, all of the results are representative of three independent experiments. The "n" indicates the number of technical replicates. $p < 0.05$ considered significant; *$p < 0.05$; **$p < 0.01$; ***$p < 0.001$ as determined by Student's t test or one-way ANOVA followed by Tukey's multiple comparisons test. Error bars represent SEMs.

to inhibit proliferation of ILC2s in a dose-dependent manner (Figure 4B). The pH of CM was in the range of 6.7–6.8, acidic compared with that of control medium (pH 7.4) (data not shown). Because of the shift in pH observed, we next sought to determine whether the inhibitory effect of CM was linked to the presence of protons. To prove this hypothesis, we buffered CM to pH 7.4 using sodium hydroxide (NaOH) and noted a significant reduction in its inhibitory effect (Figure 4C). The suppressive activity of CM was also heat stable since CM managed to inhibit the proliferation of ILC2s after prolonged boiling (Figure 4C). By Giemsa staining, we also found that ILC2s cultured in CM were smaller in size, with a scanty cytoplasm compared with those incubated in medium supplemented with IL-2 plus IL-33 and reminiscent of ILC2s cultured with IL-2 alone (Figures S5A and S5B). Apart from morphological changes, we examined the cytokine-producing capability of ILC2s. In line with its inhibitory effect on proliferation, CM significantly lowered the levels of IL-5 produced by ILC2s (Figure 4D). Quantification of ILC2s during long-term culture in CM demonstrated a roughly 3-fold decrease in the number of viable cells after 5 days, whereas an ~4-fold

increase was observed following incubation in medium supplemented with IL-2 plus IL-33 (Figure 4E). These results suggest that the suppression of proliferation, IL-5 production, and survival of ILC2s was initiated by tumor cell-derived signals reducing the pH.

Warburg observed that cancer cells preferentially convert glucose into lactate regardless of the amount of oxygen present (the eponymous "Warburg effect") (Hu et al., 2017; Koppenol et al., 2011; Vander Heiden et al., 2009; Warburg, 1956). As a result, cancer cells export lactate together with protons, which in turn lowers the pH of the tumor microenvironment. Because the suppressive activity of CM from B16F10 cells was heat stable and linked to the presence of protons, we focused on the possibility that LA is one of the factors responsible for the constraints imposed on ILC2s. To this end, we measured the level of LA in CM from B16F10 melanoma cells and found that the concentration of LA in CM was ~20 mM (±1 mM, SEM) (data not shown). In addition, we found that the level of LA significantly increased in medium from B16F10 spheroids co-cultured with ILC2s compared with B16F0 spheroids (Figure 4F). To assess the suppressive activity of LA on ILC2 proliferation, we cultured ILC2s in medium containing different concentrations of LA and sodium lactate (the latter of which does not lead to acidification of the medium) supplemented with IL-2 plus IL-33. LA was sufficient to inhibit the proliferation of ILC2s in a dose-dependent manner, whereas sodium lactate had no effect (Figure 4G). No difference in the number of proliferating ILC2s, however, was observed following culture in medium containing 20 mM LA supplemented with IL-2 only (data not shown). The addition of 20 mM LA lowered the pH of culture media from pH 7.4 to ~pH 6.0 (data not shown). To study the effect of acidification on ILC2 proliferation, we cultured ILC2s in an acidified medium (pH 6.0) prepared using hydrochloric acid (HCl) and supplemented with IL-2 plus IL-33. We noticed a significant inhibition of the proliferative potential of ILC2s, which was similar to that of 20 mM LA and was reversed after buffering the medium to pH 7.4 (Figure 4H). The inhibitory effect was dependent on the level of acidification of the medium since the number of proliferating ILC2s decreased commensurate with a decline in pH (Figure 4I). Additionally, 24 h of incubation with 20 mM LA significantly decreased the production of IL-5 as opposed to 20 mM sodium lactate (Figure 4J). The morphology of ILC2s also changed, as revealed by Giemsa staining. ILC2s incubated in medium containing 20 mM LA or HCl (pH 6.0) were smaller in size compared with those cultured in medium supplemented with IL-2 plus IL-33 and reminiscent of ILC2s incubated in medium supplemented with IL-2 alone (Figures S5C and S5D). In contrast, the addition of 20 mM sodium lactate had no effect on the morphology of ILC2s, which resembled those stimulated with IL-2 plus IL-33 (Figures S5C and S5D). Moreover, incubation of ILC2s in medium containing 20 mM LA or HCl (pH 6.0) for 24 h did not alter the surface antigen profile expressed by ILC2s, as revealed by flow cytometric analysis (Figure S5E). Nevertheless, the quantification of ILC2s exposed to medium containing 20 mM LA or HCl (pH 6.0) for 5 days demonstrated a roughly 8-fold and 2-fold decrease, respectively, in the number of viable cells (Figure 4K).

These results identify tumor cell-derived LA as one of the signals responsible for the suppression of proliferation, IL-5 production, and survival of ILC2s.

LDHA^{low} Melanoma Is More Vulnerable to Intratumoral ILC2s

To reveal the *in vivo* significance of LA, we specifically knocked down *Ldha* encoding lactate dehydrogenase A responsible for the generation of LA from pyruvic acid in B16F10 melanoma cells. We used small hairpin RNAs (shRNAs) complementary to *Ldha* to reduce its expression and established LDHA^{low} B16F10 melanoma cells. Cells transfected with unspecific, scrambled shRNA were used as controls (CTRL). The enzymatic activity of LDHA assessed by the concentration of LA in cell supernatants revealed the decreased production of lactate by LDHA^{low} cells compared with untreated and CTRL B16F10 cells (Figure S6A). No significant difference in the proliferation was observed between LDHA^{low} and CTRL cells *in vitro* (data not shown). However, subcutaneous inoculation of WT C57BL6 mice revealed that the growth of LDHA^{low} tumors was significantly delayed compared with that of CTRL tumors (Figure 5A). On day 11 post-inoculation, a larger number of Sca1^{+}KLRG1^{+} ILC2s was observed in LDHA^{low} melanomas compared with CTRL tumors (Figure 5B). In addition, LDHA^{low} tumors were enriched with CD3^{+} and CD8^{+} cells compared with CTRL tumors, further supporting the idea of the immunosuppressive activity of tumor-derived LA (Figures S6B and S6C). However, no difference was observed in the number of F4/80^{+} macrophages (Figures S6B and S6C). We next wanted to determine the effect of IL-33 on the growth of LDHA^{low} tumors. For that reason, we subcutaneously inoculated WT C57BL/6 mice with either LDHA^{low} or CTRL B16F10 cells and intraperitoneally administered IL-33 (0.5 μg in 100 μL PBS) or PBS alone at the time of inoculation and every 3 days thereafter. Intraperitoneal administration of IL-33 significantly inhibited the growth of LDHA^{low} tumors compared with CTRL tumors (Figure 5C). LDHA^{low} tumors were also typified by a massive infiltration of Sca1^{+}KLRG1^{+} ILC2s (Figure 5D). Mirroring the increase in the number of IL-33-activated ILC2s in LDHA^{low} tumors, we found an increased infiltration of eosinophils as determined by immunohistochemical analysis and quantification of MBP^{+} cells compared with CTRL tumors (Figures 5E and 5F).

Overall, these data support the idea that tumor-derived LA production negatively affects ILC2s and their antitumorigenic function in B16F10 melanoma.

LDHA Expression Correlates Negatively with Markers Associated with ILC2s in Human Cutaneous Melanomas

Since IL-33 strongly activates ILC2s, we used OncoLnc to conduct overall survival analysis for *IL33* expression in 458 human skin cutaneous melanoma (SKCM) samples from The Cancer Genome Atlas (TCGA) database (Anaya, 2016). We found that the high expression of *IL33* was associated with better overall survival ($p = 0.000535$) in melanoma patients (Figure 6A). Similarly, we found a significant correlation between overall survival in melanoma patients and the expression of an eosinophil marker *SIGLEC8* ($p = 0.000971$) (Figure 6B).

To identify the possible source of IL-33, we performed immunohistochemical analysis of sections of paraffin-embedded human control skin and cutaneous melanoma tissue samples. Although immunohistochemical analysis of control skin revealed the expression of IL-33 strictly restricted to epithelial and

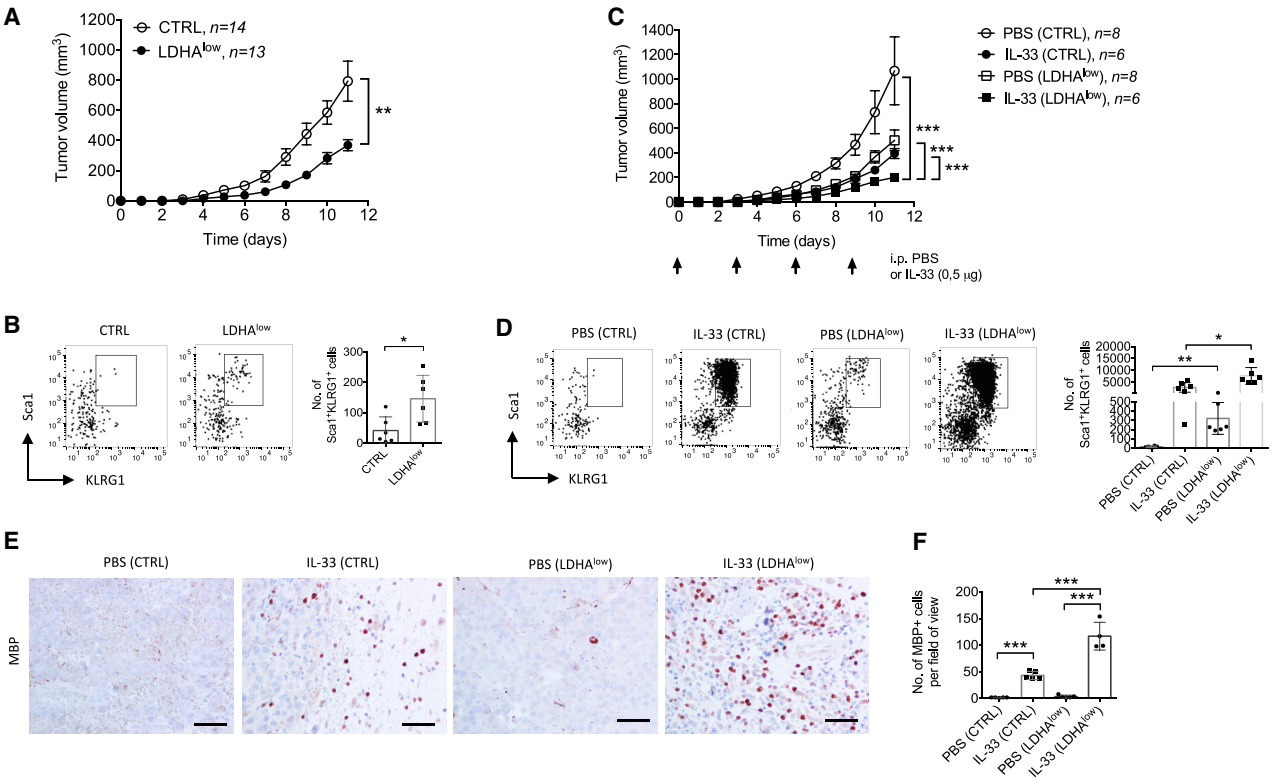

Figure 5. Inhibited LDHA-Associated LA Production *In Vivo* Improves Antitumor Efficacy of IL-33-Activated ILC2s

(A) Tumor growth profiles after subcutaneous injection of B16F10 melanoma cells with reduced expression of *LDHA* (LDHA^{low} cells) or controls (CTRL) (1 × 10^6 cells per mouse) into C57BL/6 mice (n = 13–14).

(B) Representative flow cytometry plots and quantification of ILC2 populations in the tumors (n = 6 mice per group).

(C) Growth of LDHA^{low} or CTRL cells (1 × 10^6 cells per mouse) subcutaneously injected into C57BL/6 mice (n = 6–8). The mice were subjected either to the treatment with IL-33 (0.5 μg in 100 μL PBS) or PBS at the time of tumor cell injection and every 3 days thereafter (as indicated by arrows).

(D) Representative flow cytometry plots and quantification of tumor-infiltrating ILC2s (n = 6).

(E and F) IHC analysis (E) and quantification (F) of MBP$^+$ cells present in the periphery and throughout the interior of LDHA^{low} or CTRL tumors from PBS or IL-33-treated mice (n = 4–5).

All of the results from the tumor growth studies were combined from two independent experiments. The flow cytometry results shown are from one representative experiment out of two independent experiments. The "n" indicates the number of biological replicates. $p < 0.05$ considered significant; *$p < 0.05$; **$p < 0.01$; ***$p < 0.001$ as determined by Student's t test or one-way ANOVA followed by Tukey's multiple comparisons test. The error bars represent SEMs. Mean of 5 fields of view per tumor in (F). Scale bars: 50 μm.

endothelial cells, the presence of infiltrating inflammatory cells positively stained for IL-33 typified the majority of cutaneous melanomas investigated (14 of 18 samples) (Figure 6C).

To estimate a possible genetic correlation between *IL33* and markers associated with ILC2s, we next analyzed 470 human SKCM samples from TCGA database. Although none of the markers used were completely specific to ILC2s, we found strong correlations with one another among the gene expression levels of *KLRG1*, *GATA3*, *CCR6*, *ICOS*, *KLRB1*, and *NCR3* (data not shown), which we defined here as markers associated with ILC2s. The gene expression levels of *IL33* correlated very strongly with those of markers associated with ILC2s, indicating a possible positive impact of IL-33 on tumor-infiltrating ILC2s in human melanomas (Figure 6D). Furthermore, the expression of *IL33* correlated with that of markers for eosinophils such as *SIGLEC8*, *ADGRE1*, and *ITGAM* (Figure 6E). The gene expression levels of *IL33* also correlated with *CD14* (expressed by monocytes and macrophages), as well as *CD163* and *CLEC10A* (both markers expressed by alternatively activated macrophages) (Figure 6F). Using the same database, we next estimated a possible genetic correlation between *LDHA* and markers associated with ILC2s. We found that the expression of *LDHA* negatively correlated with that of markers associated with ILC2s such as *KLRG1*, *GATA3*, *CCR6*, *ICOS*, *KLRB1*, and *NCR3* (Figure 6G). In addition, the expression of *LDHA* correlated negatively with that of markers expressed by eosinophils, including *SIGLEC8*, *ADGRE1*, and *ITGAM* (Figure 6H) and to a lesser extent, *CD14* and *CLEC10A*, but not that of *CD68* (expressed by tissue macrophages) (Figure 6I). We also found no correlation between the expression of *SIGLEC8* and *IL1RL1*. Instead, we noticed the correlation between the expression of *SIGLEC8* and genes encoding a heterodimeric receptor for IL-5, namely *IL5RA* and *CSF2RB* (Figure 6J).

These data are consistent with our findings in the mouse system and indicate that the IL-33/ILC2/eosinophil axis plays an

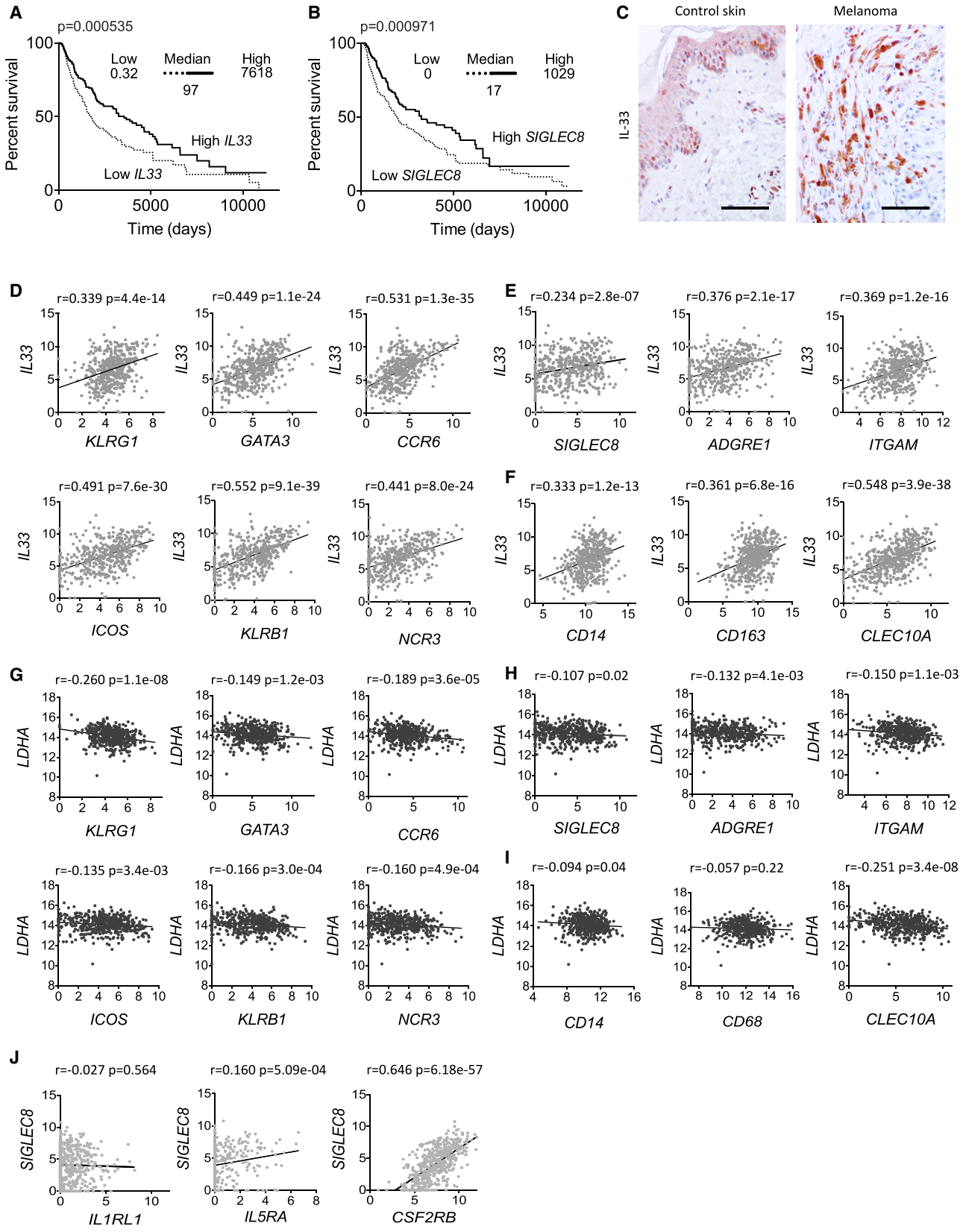

(legend on next page)

antitumorigenic role and that tumor-derived LA may have a negative effect on tumor-infiltrating ILC2s in human cutaneous melanomas.

DISCUSSION

An increased lactate production favors the progression and metastasis of various tumor types, including melanoma (Girgis et al., 2014; Walenta et al., 2000; Petrelli et al., 2015; Hirschhaeuser et al., 2011). While the metabolic reprogramming enables rapid proliferation, continuous growth, and survival of tumor cells, the ensuing accumulation of metabolites imposes considerable constraints on infiltrating immune cells (Biswas, 2015).

In this study, we unraveled an immunosuppressive axis initiated by melanoma cells on ILC2s. We showed that LA profoundly inhibited the proliferation, cytokine production, and survival of activated ILC2s *in vitro*. *In vivo* interference with LDHA function in B16F10 tumors also was sufficient to significantly increase the number of intratumoral ILC2s. In turn, ILC2s more effectively restrained the growth of LDHA^{low} B16F10 melanomas than control tumors upon IL-33 treatment. Our results corroborate and extend previous reports demonstrating that LA exerts inhibitory effects on a range of immune cells. For example, tumor-derived LA impairs the differentiation of dendritic cells (DCs) (Gottfried et al., 2006). Furthermore, LA inhibits the proliferation of and cytokine release from human T cells *in vitro*, whereas tumor lactic acidosis hinders tumor immunosurveillance by T and NK cells and their survival *in vivo* (Fischer et al., 2007; Brand et al., 2016). It has been suggested that activated T cells upregulate glycolytic metabolism, which leads to the production of LA, a process that depends on a gradient between cytoplasmic and extracellular lactate concentrations (Brand et al., 2016). Subsequently, increased concentrations of extracellular LA may facilitate its uptake, which lowers the intracellular pH in T cells and disturbs their energy metabolism, as witnessed by decreased levels of ATP (Fischer et al., 2007). Consequently, increased LA concentrations ($\geq$20 mM) cause apoptosis of T and NK cells (Fischer et al., 2007; Brand et al., 2016). In line with these observations, we found the viability of activated ILC2s substantially decreased following *in vitro* exposure to medium containing 20 mM LA or HCl (pH 6.0) for 5 days. However, tumor-associated macrophages have been found to resist the apoptosis-inducing effect of LA and acquire a protumorigenic alternatively activated phenotype (Colegio et al., 2014).

ILC2s rapidly respond to IL-33 through their expression of IL-33 receptors containing IL1RL1 (also known as ST2). IL-33 is constitutively present in the nuclei of non-hematopoietic cells, with particular abundance in certain epithelial and endothelial cell populations (Molofsky et al., 2015). Because IL-33 lacks an export signal sequence, the activation of ILC2s within the tumor microenvironment may be triggered by IL-33 passively released by necrotic and/or necroptotic cells in damaged tissues surrounding the growing tumor mass (Molofsky et al., 2015). For example, tumor-associated subcutaneous adipose tissue has been characterized by a robust infiltration of macrophages, triggered by necrosis and release of another nuclear alarmin, HMGB1 (Wagner et al., 2013; Wagner and Dudley, 2013). Of note, we found that the number of dermal adipocytes within the skin surrounding B16F10 melanomas was decreased compared with their less malignant and less invasive counterparts, B16F0 melanomas. Further analysis of tumor-associated subcutaneous adipose tissue revealed an abundance of IL-33, particularly exemplified by the presence of infiltrating inflammatory cells positively stained for IL-33. It is now clear that during inflammatory response cells of hematopoietic origin, including mast cells, DCs and macrophages actively secrete IL-33 (Furukawa et al., 2017; Schmitz et al., 2005; Mirchandani et al., 2012). Therefore, it is unlikely that the low abundance of ILC2s in B16F10 melanomas is due to the absence of signals involved in their activation.

The lack of specific immunohistochemical markers for ILC2s makes it additionally difficult to localize ILC2s within complex tissues such as tumors. However, upon IL-33 treatment, we observed lymphoid clusters in the skin surrounding implanted B16F10 melanomas. Although lymphoid clusters were present within the adjacent tissue, once incorporated into the growing tumor mass, their components will likely be exposed to the conditions within the tumor microenvironment.

The extent to which ILC2s are involved in antitumorigenic responses remains unclear, as they have been separately associated with both tumor-promoting as well as tumor-suppressing activities (Mattner and Wirtz, 2017; Wagner et al., 2017). The acquisition of antitumorigenic functions, however, seems to depend on the context of tumor specificity, justifying the reason for the use of melanoma in our study. For example, ILC2s have been implicated in the suppression of the metastatic spread of B16F10 melanoma cells within the lungs through IL-5-mediated eosinophilia (Ikutani et al., 2012). In addition, ILC2s have been shown to eliminate B16F10 melanoma cells

Figure 6. *LDHA* Expression Negatively Correlates with Markers Associated with ILC2s in Human Cutaneous Melanomas

(A and B) Overall survival of skin cutaneous melanoma (SKCM) patients generated using the OncoLnc platform. TCGA data of 458 melanoma patients were assigned into low or high groups, according to the expression level of *IL33* and *SIGLEC8* reported as RNA sequencing (RNA-seq) values. Patients having an *IL33* expression level ranging from 0.32 to 97 were considered low (dotted curve) and those having *IL33* expression level ranging from 97 to 7,618 were considered high (solid curve), whereas patients having an *SIGLEC8* expression level ranging from 0 to 17 were considered low (dotted curve) and those having an *SIGLEC8* expression level ranging from 17 to 1,029 were considered high (solid curve).

(C) IHC analysis of IL-33 expression in human control SKCM samples. Scale bars: 100 μm.

(D–F) Correlation of *IL33* with immune cells markers, including those expressed by human ILC2s (*KLRG1*, *GATA3*, *CCR6*, *ICOS*, *KLRB1*, and *NCR3*), eosinophils (*SIGLEC8*, *ADGRE1*, and *ITGAM*), and macrophages (*CD14*, *CD163*, and *CLEC10A*).

(G–I) Correlation of *LDHA* with immune cells markers, including those expressed by human ILC2s (*KLRG1*, *GATA3*, *CCR6*, *ICOS*, *KLRB1*, and *NCR3*), eosinophils (*SIGLEC8*, *ADGRE1*, and *ITGAM*), and macrophages (*CD14*, *CD68*, and *CLEC10A*).

(J) Correlation of *SIGLEC8* with *IL1RL1*, *IL5RA*, and *CSF2RB*. For correlation studies, dataset acquired from R2 platform containing 470 melanoma patients (tumor SKCM–TCGA–470–rsem–tcgars) was used. Pearson's correlation coefficient, r, is shown.

genetically engineered to express IL-33 (Kim et al., 2016). It should be noted, however, that those studies did not focus on intratumoral ILC2s or rely on a chronic and non-physiological production of IL-33 by transgenic melanoma cells, which significantly alters the number of ILC2s in the course of tumor development. ILC2s may exert their antitumorigenic function through various means. In tumors engineered to express IL-33, including B16F10 melanomas, infiltration of ILC2s has drastically reduced the tumor growth and induced tumor-cell specific apoptosis (Kim et al., 2016). In addition, ILC2s adoptively transferred into *Rag2*$^{-/-}$*Il2rg*$^{-/-}$ mice inhibited the growth of EL4 lymphomas expressing IL-33 through CXCR2 signaling (Kim et al., 2016). In our model, we observed the growth of B16F10 melanomas similarly delayed following co-injection with ILC2s with tumors typified by an increased number of eosinophils. It remains to be deciphered, however, to what extent ILC2s contribute to the induction of tumor-cell specific apoptosis.

In addition to immunosuppressive cytokines such as IL-4 and IL-13, ILC2s produce high levels of IL-5 (Moro et al., 2010). IL-5 is essential for the expansion of eosinophils, since its localized production induces tissue eosinophilia (Sanderson et al., 1985; Leitch et al., 2009; Rosenberg et al., 2013). An increased incidence of methylcholanthrene (MCA)-induced fibrosarcomas has been observed in the eosinophil-deficient *IL-5*$^{-/-}$*CCL11*$^{-/-}$ and ΔdblGATA mice, and this correlated with their reduced number in the tumors (Simson et al., 2007). Conversely, MCA-induced tumor incidence and growth have been significantly suppressed in IL-5-overexpressing transgenic mice associated with robust eosinophilia in the periphery and throughout the interior of the tumors (Simson et al., 2007). Of note, the cytotoxic activity of eosinophils has been ascribed to the secretory granules composed of MBP-1 and MBP-2, eosinophil cationic protein, eosin-derived neurotoxin, and eosinophil peroxidase (Davis and Rothenberg, 2014). For example, MBP^{+} eosinophils have been found to be critical in the clearance of metastatic B16F10 cells in the lungs, whereas the lysates of eosinophils become cytotoxic when cultured with melanoma cells (Mattes et al., 2003).

In our model, B16F10 tumors were typified by an increased infiltration of ILC2s and eosinophils, following IL-33 treatment. Therefore, the suppressing effect on tumor growth, which we observed, may be related, in part, to the presence of eosinophils. Concordantly with this hypothesis, Lucarini et al. (2017) reported that both B16F10 melanoma growth and metastasis formation were enhanced upon *in vivo* depletion of eosinophils using an anti-Siglec-F antibody. Eosinophils have also been found to enable T cell responses through the normalization of the tumor vasculature (Carretero et al., 2016). However, we did not observe a significant increase in the number of T cells at the time of sacrifice, suggesting that we either failed to generate a sufficient adaptive immune response against implanted melanoma cells during the course of the experiment or that adaptive immunity was not involved. The growth of B16F10 tumors has been found to be greatly impaired following IL-33 treatment of *Rag1*$^{-/-}$ mice, which indicates that the systemic administration of IL-33 can inhibit melanoma growth solely through the innate immune system (Long et al., 2018). It has also been revealed that the depletion of lymphoid cells such as CD4^{+} T cells, CD8^{+} T cells, or NK cells using anti-CD4, anti-CD8, and anti-ASGM1 antibodies (which may also target other cell types, including macrophages; Wiltrout et al., 1985), respectively, does not affect the growth of B16F10 melanomas and EL4 lymphomas engineered to express IL-33 (Kim et al., 2016). Similarly, we found no difference in the growth of B16F10 melanomas between Rag2$^{-/-}$ mice depleted of NK cells using anti-ASGM1 antibodies and Rag2$^{-/-}$ mice that received control IgG during IL-33 treatment. In contrast, Dominguez et al. (2017) have found that the growth of B16F10 tumors is inhibited in a CD8^{+} T cell-dependent manner (but a CD4^{+} T cell- and NK cell-independent manner) following treatment with the IL-33 of mice with already established tumors. One way to reconcile these contradictory features of IL-33 could be to recognize the role of the IL-33 concentration in the tumor microenvironment and the mode and length of administration.

In the skin surrounding the tumors, we noticed an increased number of macrophages typified as alternatively activated by the expression of CD301 (Biswas and Mantovani, 2012). It has already been found that IL-33/ST2 signaling amplifies the proliferation and polarization of alternatively activated macrophages (Kurowska-Stolarska et al., 2009; Jackson-Jones et al., 2016). It has also been shown that alternatively activated macrophages suppress T cell expansion, which could in part explain the lack of increased T cell responsiveness in our model (Taylor et al., 2006; Schebesch et al., 1997; Huber et al., 2010; Nair et al., 2009). Therefore, it is tempting to speculate whether selective depletion of alternatively activated macrophages could further tip the scales toward a microenvironment that impedes tumor growth, especially since some tissue-resident macrophages are relatively long-lived cells (Shaw et al., 2018). Of no less importance is the fact that we abstained from using the ovalbumin-expressing melanoma cells frequently used to augment tumor-specific adaptive immune responses.

Several immunotherapeutic strategies to treat cancer patients appear to be dependent upon the preexistence of an immune infiltrate (Spranger et al., 2015; Ji et al., 2012; Tumeh et al., 2014). Using a cohort of 458 cutaneous skin melanoma patients, we demonstrated that the expression of *IL33* and *SIGLEC8* is associated with better overall survival. The expression of *IL33* correlated positively, whereas that of *LDHA* correlated negatively with markers associated with human ILC2s and eosinophils. Therefore, our results indicate that the expression of *LDHA* may serve as a predictive marker of ILC2 infiltration in human melanomas. It should also be noted, however, that no correlation was observed between the expression levels of *IL33* and *SIGLEC8* and overall survival for some other tumors such as lung squamous cell carcinoma and pancreatic adenocarcinoma (data not shown), suggesting that the antitumor activity of ILC2s is tumor-type specific.

It remains to be deciphered how other metabolic factors and hypoxia affect ILC2s within the tumor microenvironment (Wagner and Koyasu, 2019). Our results identify the tumor-derived LA production as a plausible immunosuppressive mechanism that contributes to the paucity of intratumoral ILC2s. With an increasing understanding of the immune system, it remains to be seen to what extent the antitumorigenic potential of ILC2s can be used for the development of new immunotherapies.

STAR★METHODS

Detailed methods are provided in the online version of this paper and include the following:

- KEY RESOURCES TABLE
- LEAD CONTACT AND MATERIALS AVAILABILITY
- EXPERIMENTAL MODEL AND SUBJECT DETAILS
  - Mice
  - Cells and Complete Media
  - Human Samples
- METHOD DETAILS
  - Tumor Cell Implantation
  - Conditioned Medium Preparation
  - Hanging Drop Culture for Spheroid Formation and Co-Culture with ILC2s
  - MTS Proliferation Assay
  - Measurements of IL-5
  - Measurements of Lactic Acid
  - Giemsa Staining
  - Immunohistochemistry
  - Picrosirius Red Staining
  - Flow Cytometry
- QUANTIFICATION AND STATISTICAL ANALYSIS
  - Database Analysis
  - Statistics
- DATA AND CODE AVAILABITY

SUPPLEMENTAL INFORMATION

Supplemental Information can be found online at https://doi.org/10.1016/j.celrep.2020.01.103.

ACKNOWLEDGMENTS

We thank I. Pryme for critical reading of the manuscript; T. Shitamichi, S. Tada, N. Hagiwara, and Y. Sasako for animal care; members of the animal facility and the fluorescence-activated cell sorting (FACS) platform for technical support; and members of the Laboratory for Innate Immune Systems for valuable discussions. This work was supported by a research grant in connection with a stay abroad and Legat for Forskning av Kreftsykdommer (814172) from the University of Bergen, Norway, to M.W., and by a Grant-in-Aid for Scientific Research (A) (16H02631) from the Japan Society for the Promotion of Science, to S.K.

AUTHOR CONTRIBUTIONS

Conceptualization, M.W. and S.K.; Methodology, M.W., T.K., H.T., K.N.E., Y.M., K.M., and S.K.; Investigation, M.W., T.K., and H.T.; Formal Analysis, M.W.; Writing – Original Draft, M.W. and S.K.; Writing – Review & Editing, M.W., T.K., H.T., K.N.E., Y.M., K.M., and S.K.; Funding Acquisition, M.W. and S.K.; Resources, K.M. and S.K.; Supervision, M.W., K.M., and S.K.

DECLARATION OF INTERESTS

The authors declare no competing interests.

Received: February 4, 2019
Revised: July 18, 2019
Accepted: January 29, 2020
Published: February 25, 2020

REFERENCES

Anaya, J. (2016). OncoLnc: linking TCGA survival data to mRNAs, miRNAs, and lncRNAs. PeerJ Comput. Sci. *2*, e67.

Artis, D., and Spits, H. (2015). The biology of innate lymphoid cells. Nature *517*, 293–301.

Biswas, S.K. (2015). Metabolic Reprogramming of Immune Cells in Cancer Progression. Immunity *43*, 435–449.

Biswas, S.K., and Mantovani, A. (2012). Orchestration of metabolism by macrophages. Cell Metab. *15*, 432–437.

Brand, A., Singer, K., Koehl, G.E., Kolitzus, M., Schoenhammer, G., Thiel, A., Matos, C., Bruss, C., Klobuch, S., Peter, K., et al. (2016). LDHA-Associated Lactic Acid Production Blunts Tumor Immunosurveillance by T and NK Cells. Cell Metab. *24*, 657–671.

Brestoff, J.R., Kim, B.S., Saenz, S.A., Stine, R.R., Monticelli, L.A., Sonnenberg, G.F., Thome, J.J., Farber, D.L., Lutfy, K., Seale, P., and Artis, D. (2015). Group 2 innate lymphoid cells promote beiging of white adipose tissue and limit obesity. Nature *519*, 242–246.

Carrega, P., Loiacono, F., Di Carlo, E., Scaramuccia, A., Mora, M., Conte, R., Benelli, R., Spaggiari, G.M., Cantoni, C., Campana, S., et al. (2015). NCR(+) ILC3 concentrate in human lung cancer and associate with intratumoral lymphoid structures. Nat. Commun. *6*, 8280.

Carretero, R., Sektioglu, I.M., Garbi, N., Salgado, O.C., Beckhove, P., and Hammerling, G.J. (2016). Eosinophils orchestrate cancer rejection by normalizing tumor vessels and enhancing infiltration of CD8(+) T cells (vol 16, pg 609, 2015). Nat. Immunol. *17*, 214.

Cephus, J.Y., Stier, M.T., Fuseini, H., Yung, J.A., Toki, S., Bloodworth, M.H., Zhou, W., Goleniewska, K., Zhang, J., Garon, S.L., et al. (2017). Testosterone Attenuates Group 2 Innate Lymphoid Cell-Mediated Airway Inflammation. Cell Rep. *21*, 2487–2499.

Chang, C.H., Qiu, J., O'Sullivan, D., Buck, M.D., Noguchi, T., Curtis, J.D., Chen, Q., Gindin, M., Gubin, M.M., Van Der Windt, G.J., et al. (2015). Metabolic Competition in the Tumor Microenvironment Is a Driver of Cancer Progression. Cell *162*, 1229–1241.

Colegio, O.R., Chu, N.Q., Szabo, A.L., Chu, T., Rhebergen, A.M., Jairam, V., Cyrus, N., Brokowski, C.E., Eisenbarth, S.C., Phillips, G.M., et al. (2014). Functional polarization of tumour-associated macrophages by tumour-derived lactic acid. Nature *513*, 559–563.

Davis, B.P., and Rothenberg, M.E. (2014). Eosinophils and cancer. Cancer Immunol. Res. *2*, 1–8.

Doherty, J.R., and Cleveland, J.L. (2013). Targeting lactate metabolism for cancer therapeutics. J. Clin. Invest. *123*, 3685–3692.

Dominguez, D., Ye, C., Geng, Z., Chen, S., Fan, J., Qin, L., Long, A., Wang, L., Zhang, Z., Zhang, Y., et al. (2017). Exogenous IL-33 Restores Dendritic Cell Activation and Maturation in Established Cancer. J. Immunol. *198*, 1365–1375.

Ealey, K.N., Moro, K., and Koyasu, S. (2017). Are ILC2s Jekyll and Hyde in airway inflammation? Immunol. Rev. *278*, 207–218.

Ebbo, M., Crinier, A., Vely, F., and Vivier, E. (2017). Innate lymphoid cells: major players in inflammatory diseases. Nat. Rev. Immunol. *17*, 665–678.

Fischer, K., Hoffmann, P., Voelkl, S., Meidenbauer, N., Ammer, J., Edinger, M., Gottfried, E., Schwarz, S., Rothe, G., Hoves, S., et al. (2007). Inhibitory effect of tumor cell-derived lactic acid on human T cells. Blood *109*, 3812–3819.

Furukawa, S., Moriyama, M., Miyake, K., Nakashima, H., Tanaka, A., Maehara, T., Iizuka-Koga, M., Tsuboi, H., Hayashida, J.N., Ishiguro, N., et al. (2017). Interleukin-33 produced by M2 macrophages and other immune cells contributes to Th2 immune reaction of IgG4-related disease. Sci. Rep. *7*, 42413.

Furusawa, J., Moro, K., Motomura, Y., Okamoto, K., Zhu, J., Takayanagi, H., Kubo, M., and Koyasu, S. (2013). Critical role of p38 and GATA3 in natural helper cell function. J. Immunol. *191*, 1818–1826.

Gajewski, T.F., Schreiber, H., and Fu, Y.X. (2013). Innate and adaptive immune cells in the tumor microenvironment. Nat. Immunol. *14*, 1014–1022.

Gatenby, R.A., and Gillies, R.J. (2004). Why do cancers have high aerobic glycolysis? Nat. Rev. Cancer *4*, 891–899.

Girgis, H., Masui, O., White, N.M., Scorilas, A., Rotondo, F., Seivwright, A., Gabril, M., Filter, E.R., Girgis, A.H., Bjarnason, G.A., et al. (2014). Lactate dehydrogenase A is a potential prognostic marker in clear cell renal cell carcinoma. Mol. Cancer *13*, 101.

Gottfried, E., Kunz-Schughart, L.A., Ebner, S., Mueller-Klieser, W., Hoves, S., Andreesen, R., Mackensen, A., and Kreutz, M. (2006). Tumor-derived lactic acid modulates dendritic cell activation and antigen expression. Blood *107*, 2013–2021.

Hammad, H., and Lambrecht, B.N. (2015). Barrier Epithelial Cells and the Control of Type 2 Immunity. Immunity *43*, 29–40.

Hay, N. (2016). Reprogramming glucose metabolism in cancer: can it be exploited for cancer therapy? Nat. Rev. Cancer *16*, 635–649.

Hirschhaeuser, F., Sattler, U.G., and Mueller-Klieser, W. (2011). Lactate: a metabolic key player in cancer. Cancer Res. *71*, 6921–6925.

Hu, X., Chao, M., and Wu, H. (2017). Central role of lactate and proton in cancer cell resistance to glucose deprivation and its clinical translation. Signal Transduct. Target. Ther. *2*, 16047.

Huber, S., Hoffmann, R., Muskens, F., and Voehringer, D. (2010). Alternatively activated macrophages inhibit T-cell proliferation by Stat6-dependent expression of PD-L2. Blood *116*, 3311–3320.

Ikutani, M., Yanagibashi, T., Ogasawara, M., Tsuneyama, K., Yamamoto, S., Hattori, Y., Kouro, T., Itakura, A., Nagai, Y., Takaki, S., and Takatsu, K. (2012). Identification of innate IL-5-producing cells and their role in lung eosinophil regulation and antitumor immunity. J. Immunol. *188*, 703–713.

Jackson-Jones, L.H., Ruckerl, D., Svedberg, F., Duncan, S., Maizels, R.M., Sutherland, T.E., Jenkins, S.J., Mcsorley, H.J., Benezech, C., Macdonald, A.S., and Allen, J.E. (2016). IL-33 delivery induces serous cavity macrophage proliferation independent of interleukin-4 receptor alpha. Eur. J. Immunol. *46*, 2311–2321.

Ji, R.R., Chasalow, S.D., Wang, L., Hamid, O., Schmidt, H., Cogswell, J., Alaparthy, S., Berman, D., Jure-Kunkel, M., Siemers, N.O., et al. (2012). An immune-active tumor microenvironment favors clinical response to ipilimumab. Cancer Immunol. Immunother. *61*, 1019–1031.

Kabata, H., Moro, K., Fukunaga, K., Suzuki, Y., Miyata, J., Masaki, K., Betsuyaku, T., Koyasu, S., and Asano, K. (2013). Thymic stromal lymphopoietin induces corticosteroid resistance in natural helper cells during airway inflammation. Nat. Commun. *4*, 2675.

Kabata, H., Moro, K., and Koyasu, S. (2018). The group 2 innate lymphoid cell (ILC2) regulatory network and its underlying mechanisms. Immunol. Rev. *286*, 37–52.

Kim, J., Kim, W., Moon, U.J., Kim, H.J., Choi, H.J., Sin, J.I., Park, N.H., Cho, H.R., and Kwon, B. (2016). Intratumorally Establishing Type 2 Innate Lymphoid Cells Blocks Tumor Growth. J. Immunol. *196*, 2410–2423.

Koppenol, W.H., Bounds, P.L., and Dang, C.V. (2011). Otto Warburg's contributions to current concepts of cancer metabolism. Nat. Rev. Cancer *11*, 325–337.

Kurowska-Stolarska, M., Stolarski, B., Kewin, P., Murphy, G., Corrigan, C.J., Ying, S., Pitman, N., Mirchandani, A., Rana, B., Van Rooijen, N., et al. (2009). IL-33 amplifies the polarization of alternatively activated macrophages that contribute to airway inflammation. J. Immunol. *183*, 6469–6477.

Leitch, V.D., Strudwick, X.L., Matthaei, K.I., Dent, L.A., and Cowin, A.J. (2009). IL-5-overexpressing mice exhibit eosinophilia and altered wound healing through mechanisms involving prolonged inflammation. Immunol. Cell Biol. *87*, 131–140.

Long, A., Dominguez, D., Qin, L., Chen, S., Fan, J., Zhang, M., Fang, D., Zhang, Y., Kuzel, T.M., and Zhang, B. (2018). Type 2 Innate Lymphoid Cells Impede IL-33-Mediated Tumor Suppression. J. Immunol. *201*, 3456–3464.

Lucarini, V., Zicchedda, G., Macchia, I., La Sorsa, V., Peschiaroli, F., Buccione, C., Sistigu, A., Sanchez, M., Andreone, S., D'Urso, M.T., et al. (2017). IL-33 restricts tumor growth and inhibits pulmonary metastasis in melanoma-bearing mice through eosinophils. Oncoimmunology *6*, e1317420.

Lund, A.W., Wagner, M., Fankhauser, M., Steinskog, E.S., Broggi, M.A., Sprenger, S., Gajewski, T.F., Alitalo, K., Eikesdal, H.P., Wiig, H., and Swartz, M.A. (2016). Lymphatic vessels regulate immune microenvironments in human and murine melanoma. J. Clin. Invest. *126*, 3389–3402.

Lyssiotis, C.A., and Kimmelman, A.C. (2017). Metabolic Interactions in the Tumor Microenvironment. Trends Cell Biol. *27*, 863–875.

Mattes, J., Hulett, M., Xie, W., Hogan, S., Rothenberg, M.E., Foster, P., and Parish, C. (2003). Immunotherapy of cytotoxic T cell-resistant tumors by T helper 2 cells: an eotaxin and STAT6-dependent process. J. Exp. Med. *197*, 387–393.

Mattner, J., and Wirtz, S. (2017). Friend or Foe? The Ambiguous Role of Innate Lymphoid Cells in Cancer Development. Trends Immunol. *38*, 29–38.

Mirchandani, A.S., Salmond, R.J., and Liew, F.Y. (2012). Interleukin-33 and the function of innate lymphoid cells. Trends Immunol. *33*, 389–396.

Mjosberg, J., Bernink, J., Golebski, K., Karrich, J.J., Peters, C.P., Blom, B., Te Velde, A.A., Fokkens, W.J., Van Drunen, C.M., and Spits, H. (2012). The transcription factor GATA3 is essential for the function of human type 2 innate lymphoid cells. Immunity *37*, 649–659.

Mohapatra, A., Van Dyken, S.J., Schneider, C., Nussbaum, J.C., Liang, H.E., and Locksley, R.M. (2016). Group 2 innate lymphoid cells utilize the IRF4-IL-9 module to coordinate epithelial cell maintenance of lung homeostasis. Mucosal Immunol. *9*, 275–286.

Molofsky, A.B., Savage, A.K., and Locksley, R.M. (2015). Interleukin-33 in Tissue Homeostasis, Injury, and Inflammation. Immunity *42*, 1005–1019.

Moro, K., Yamada, T., Tanabe, M., Takeuchi, T., Ikawa, T., Kawamoto, H., Furusawa, J., Ohtani, M., Fujii, H., and Koyasu, S. (2010). Innate production of T(H)2 cytokines by adipose tissue-associated c-Kit(+)Sca-1(+) lymphoid cells. Nature *463*, 540–544.

Moro, K., Ealey, K.N., Kabata, H., and Koyasu, S. (2015). Isolation and analysis of group 2 innate lymphoid cells in mice. Nat. Protoc. *10*, 792–806.

Moro, K., Kabata, H., Tanabe, M., Koga, S., Takeno, N., Mochizuki, M., Fukunaga, K., Asano, K., Betsuyaku, T., and Koyasu, S. (2016). Interferon and IL-27 antagonize the function of group 2 innate lymphoid cells and type 2 innate immune responses. Nat. Immunol. *17*, 76–86.

Nair, M.G., Du, Y., Perrigoue, J.G., Zaph, C., Taylor, J.J., Goldschmidt, M., Swain, G.P., Yancopoulos, G.D., Valenzuela, D.M., Murphy, A., et al. (2009). Alternatively activated macrophage-derived RELM-{alpha} is a negative regulator of type 2 inflammation in the lung. J. Exp. Med. *206*, 937–952.

Neill, D.R., Wong, S.H., Bellosi, A., Flynn, R.J., Daly, M., Langford, T.K., Bucks, C., Kane, C.M., Fallon, P.G., Pannell, R., et al. (2010). Nuocytes represent a new innate effector leukocyte that mediates type-2 immunity. Nature *464*, 1367–1370.

Petrelli, F., Cabiddu, M., Coinu, A., Borgonovo, K., Ghilardi, M., Lonati, V., and Barni, S. (2015). Prognostic role of lactate dehydrogenase in solid tumors: a systematic review and meta-analysis of 76 studies. Acta Oncol. *54*, 961–970.

Price, A.E., Liang, H.E., Sullivan, B.M., Reinhardt, R.L., Eisley, C.J., Erle, D.J., and Locksley, R.M. (2010). Systemically dispersed innate IL-13-expressing cells in type 2 immunity. Proc. Natl. Acad. Sci. USA *107*, 11489–11494.

Rosenberg, H.F., Dyer, K.D., and Foster, P.S. (2013). Eosinophils: changing perspectives in health and disease. Nat. Rev. Immunol. *13*, 9–22.

Sanderson, C.J., Warren, D.J., and Strath, M. (1985). Identification of a Lymphokine That Stimulates Eosinophil Differentiation Invitro - Its Relationship to Interleukin-3, and Functional-Properties of Eosinophils Produced in Cultures. J. Exp. Med. *162*, 60–74.

Sasaki, T., Moro, K., Kubota, T., Kubota, N., Kato, T., Ohno, H., Nakae, S., Saito, H., and Koyasu, S. (2019). Innate Lymphoid Cells in the Induction of Obesity. Cell Rep. *28*, 202–217.

Schebesch, C., Kodelja, V., Muller, C., Hakij, N., Bisson, S., Orfanos, C.E., and Goerdt, S. (1997). Alternatively activated macrophages actively inhibit proliferation of peripheral blood lymphocytes and CD4+ T cells in vitro. Immunology *92*, 478–486.

Schmitz, J., Owyang, A., Oldham, E., Song, Y., Murphy, E., Mcclanahan, T.K., Zurawski, G., Moshrefi, M., Qin, J., Li, X., et al. (2005). IL-33, an interleukin-1-

like cytokine that signals via the IL-1 receptor-related protein ST2 and induces T helper type 2-associated cytokines. Immunity *23*, 479–490.

Shaw, T.N., Houston, S.A., Wemyss, K., Bridgeman, H.M., Barbera, T.A., Zangerle-Murray, T., Strangward, P., Ridley, A.J.L., Wang, P., Tamoutounour, S., et al. (2018). Tissue-resident macrophages in the intestine are long lived and defined by Tim-4 and CD4 expression. J. Exp. Med. *215*, 1507–1518.

Simson, L., Ellyard, J.I., Dent, L.A., Matthaei, K.I., Rothenberg, M.E., Foster, P.S., Smyth, M.J., and Parish, C.R. (2007). Regulation of carcinogenesis by IL-5 and CCL11: a potential role for eosinophils in tumor immune surveillance. J. Immunol. *178*, 4222–4229.

Spits, H., Artis, D., Colonna, M., Diefenbach, A., Di Santo, J.P., Eberl, G., Koyasu, S., Locksley, R.M., Mckenzie, A.N., Mebius, R.E., et al. (2013). Innate lymphoid cells–a proposal for uniform nomenclature. Nat. Rev. Immunol. *13*, 145–149.

Spranger, S., Bao, R., and Gajewski, T.F. (2015). Melanoma-intrinsic beta-catenin signalling prevents anti-tumour immunity. Nature *523*, 231–235.

Steinskog, E.S.S., Sagstad, S.J., Wagner, M., Karlsen, T.V., Yang, N., Markhus, C.E., Yndestad, S., Wiig, H., and Eikesdal, H.P. (2016). Impaired lymphatic function accelerates cancer growth. Oncotarget *7*, 45789–45802.

Taylor, M.D., Harris, A., Nair, M.G., Maizels, R.M., and Allen, J.E. (2006). F4/80+ alternatively activated macrophages control CD4+ T cell hyporesponsiveness at sites peripheral to filarial infection. J. Immunol. *176*, 6918–6927.

Tumeh, P.C., Harview, C.L., Yearley, J.H., Shintaku, I.P., Taylor, E.J., Robert, L., Chmielowski, B., Spasic, M., Henry, G., Ciobanu, V., et al. (2014). PD-1 blockade induces responses by inhibiting adaptive immune resistance. Nature *515*, 568–571.

Vander Heiden, M.G., Cantley, L.C., and Thompson, C.B. (2009). Understanding the Warburg effect: the metabolic requirements of cell proliferation. Science *324*, 1029–1033.

Vivier, E., Van De Pavert, S.A., Cooper, M.D., and Belz, G.T. (2016). The evolution of innate lymphoid cells. Nat. Immunol. *17*, 790–794.

Vivier, E., Artis, D., Colonna, M., Diefenbach, A., Di Santo, J.P., Eberl, G., Koyasu, S., Locksley, R.M., Mckenzie, A.N.J., Mebius, R.E., et al. (2018). Innate Lymphoid Cells: 10 Years On. Cell *174*, 1054–1066.

Von Moltke, J., Ji, M., Liang, H.E., and Locksley, R.M. (2016). Tuft-cell-derived IL-25 regulates an intestinal ILC2-epithelial response circuit. Nature *529*, 221–225.

Wagner, M., and Dudley, A.C. (2013). A three-party alliance in solid tumors: adipocytes, macrophages and vascular endothelial cells. Adipocyte *2*, 67–73.

Wagner, M., and Koyasu, S. (2019). Cancer Immunoediting by Innate Lymphoid Cells. Trends Immunol. *40*, 415–430.

Wagner, M., Bjerkvig, R., Wiig, H., Melero-Martin, J.M., Lin, R.Z., Klagsbrun, M., and Dudley, A.C. (2012). Inflamed tumor-associated adipose tissue is a depot for macrophages that stimulate tumor growth and angiogenesis. Angiogenesis *15*, 481–495.

Wagner, M., Bjerkvig, R., Wiig, H., and Dudley, A.C. (2013). Loss of adipocyte specification and necrosis augment tumor-associated inflammation. Adipocyte *2*, 176–183.

Wagner, M., Moro, K., and Koyasu, S. (2017). Plastic Heterogeneity of Innate Lymphoid Cells in Cancer. Trends Cancer *3*, 326–335.

Walenta, S., Wetterling, M., Lehrke, M., Schwickert, G., Sundfor, K., Rofstad, E.K., and Mueller-Klieser, W. (2000). High lactate levels predict likelihood of metastases, tumor recurrence, and restricted patient survival in human cervical cancers. Cancer Res. *60*, 916–921.

Warburg, O. (1956). On the origin of cancer cells. Science *123*, 309–314.

Wiltrout, R.H., Santoni, A., Peterson, E.S., Knott, D.C., Overton, W.R., Herberman, R.B., and Holden, H.T. (1985). Reactivity of anti-asialo GM1 serum with tumoricidal and non-tumoricidal mouse macrophages. J. Leukoc. Biol. *37*, 597–614.

STAR★METHODS

KEY RESOURCES TABLE

REAGENT or RESOURCE	SOURCE	IDENTIFIER
Antibodies		
Anti-mouse LYVE1	Abcam	Catalog# ab14917; RRID:AB_301509
Anti-mouse CD31	Santa Cruz Biotechnology	Catalog# sc1506; RRID:AB_2161037
Anti-mouse Perilipin1 (D1D8)	Cell Signaling Technology	Catalog# 9349; RRID:AB_10829911
Anti-mouse CD3 (CD3-12)	Abcam	Catalog# ab11089; RRID:AB_369097
Anti-mouse CD8 (EPR21769)	Abcam	Catalog# ab217344
Anti-mouse CD4 (EPR19514)	Abcam	Catalog# ab183685; RRID:AB_2686917
Anti-mouse CD11b	Abcam	Catalog# ab75476; RRID:AB_1310048
Anti-mouse F4/80 (CI:A3-1)	Abcam	Catalog# ab6640; RRID:AB_1140040
Anti-mouse CD301 (ER-MP23)	Bio-Rad	Catalog# MCA2392; RRID:AB_872014
Anti-mouse MBP (AA100-215)	Antibodies online	Catalog# ABIN1174871
Anti-mouse IL-33	Cloud-Clone Corp	Catalog# PAB980Mu01
Anti-human IL-33	R&D Systems	Catalog# MAB36252
Anti-rabbit IgG (H+L), Biotin-conjugated	Vector Laboratories	Catalog# BA-1000
Anti-rat IgG (H+L), Biotin-conjugated	Vector Laboratories	Catalog# BA-4000
Anti-goat IgG (H+L), Biotin-conjugated	Vector Laboratories	Catalog# BA-5000
Anti-mouse Ly6A/E (Sca1) (D7), BV421-conjugated	BD Biosciences	Catalog# 562729; RRID:AB_2737750
Anti-mouse Ly6A/E (Sca1) (E13-161.7), FITC-conjugated	BD Biosciences	Catalog# 553335; RRID:AB_394791
Anti-mouse KLRG1 (2F1), APC-conjugated	BD Biosciences	Catalog# 561620; RRID:AB_10895798
Anti-mouse CD45.2 (104), PE-conjugated	BD Biosciences	Catalog# 560695; RRID:AB_1727493
Anti-mouse c-Kit (2B8), PE/Cy7-conjugated	BD Biosciences	Catalog# 558163; RRID:AB_647250
Anti-mouse Thy1.2 (53-2.1), V500-conjugated	BD Biosciences	Catalog# 561616; RRID:AB_10894013
Anti-mouse T1/ST2 (DJ8), FITC-conjugated	BD Biosciences	Catalog# 101001F; RRID:AB_10718414
Anti-mouse CD25, APC/Cy7-conjugated	BD Biosciences	Catalog# 557658; RRID: AB_396773
Anti-mouse Siglec-F (E50-2440), BV421-conjugated	BD Biosciences	Catalog# 562681; RRID: AB_2722581
Anti-mouse CD11b (M1/70), APC-conjugated	BD Biosciences	Catalog# 553312; RRID: AB_398535
Anti-mouse NK1.1 (PK136), FITC-conjugated	BD Biosciences	Catalog# 553164; RRID: AB_394676
Anti-mouse CD3ε (145-2C11), APC-conjugated	BD Biosciences	Catalog# 553066; RRID: AB_398529
Anti-mouse CD45.2 (104), APC/Cy7-conjugated	BD Biosciences	Catalog# 560694; RRID: AB_1727492
Anti-mouse CD3ε (145-2C11), Biotin-conjugated	BD Biosciences	Catalog# 553060; RRID:AB_394593
Anti-mouse CD8α (53-6.7), Biotin-conjugated	BD Biosciences	Catalog# 553029; RRID:AB_394567
Anti-mouse CD4 (GK1.5), Biotin-conjugated	BD Biosciences	Catalog# 553728; RRID:AB_395012
Anti-mouse CD11c (HL3), Biotin-conjugated	BD Biosciences	Catalog# 553800; RRID:AB_395059
Anti-mouse FcεRIα (MAR-1), Biotin-conjugated	BioLegend	Catalog# 134304; RRID:AB_1626106
Anti- mouse NK1.1 (PK136), Biotin-conjugated	BD Biosciences	Catalog# 553163; RRID:AB_394675
Anti-mouse CD19 (1D3), Biotin-conjugated	BD Biosciences	Catalog# 553784; RRID:AB_395048
Anti-mouse CD11b (M1/70), Biotin-conjugated	BD Biosciences	Catalog# 553309; RRID:AB_394773
Anti-mouse TER119 (TER119), Biotin-conjugated	BD Biosciences	Catalog# 553672; RRID:AB_394985
Anti-mouse GR1 (R86-8C5), Biotin-conjugated	BD Biosciences	Catalog# 553125; RRID:AB_394641
Anti-mouse CD5 (53-7.3), Biotin-conjugated	BD Biosciences	Catalog# 553019; RRID:AB_394557
Streptavidin, V500-conjugated	BD Biosciences	Catalog# 561419; RRID:AB_10611863
Streptavidin, APC-conjugated	BD Biosciences	Catalog# 554067; RRID:AB_10050396
Anti-mouse CD16/32 (2.4G2), purified	Hybridoma	N/A

(*Continued on next page*)

Continued

REAGENT or RESOURCE	SOURCE	IDENTIFIER
Anti-mouse ASGM1, rabbit	Fujifilm Wako	Catalog# 014-09801
Rabbit IgG Control Antibody, Unconjugated	Sigma-Aldrich	Catalog# I8140; RRID: AB_1163661
Biological Samples		
Human malignant melanoma tissue array	US Biomax; https://www.biomax.us	Catalog# ME803b
Chemicals, Peptides, and Recombinant Proteins		
PI (propidium iodide)	Sigma-Aldrich	Catalog# 81845
L-(+)-Lactic acid	Sigma-Aldrich	Catalog# L1750
Sodium L-lactate	Sigma-Aldrich	Catalog# L7022
Recombinant Mouse IL-2 Protein	R&D Systems	Catalog# 402-ML
Recombinant Mouse IL-33 Protein	R&D Systems	Catalog# 3626-ML
Proteinase K	Dako	Catalog# S3020
Vectastain® Elite® ABC HRP Reagent	Vector Laboratories	Catalog# PK-7100
Liquid DAB+ Substrate Chromogen System	Dako	Catalog# K3468
Entellan®	Merck	Catalog# 107960
Corning Cell-Tak Cell and Tissue Adhesive	Thermo Fisher Scientific	Catalog# 354240
Liberase TH	Roche	Catalog# 5401135001
Collagenase D	Roche	Catalog# 11088858001
Critical Commercial Assays		
CellTiter 96® AQueous One Solution Cell Proliferation Assay (MTS)	Promega	Catalog# G3580
L-Lactate Assay Kit	Abcam	Catalog# ab65331
Mouse IL-5 Platinum ELISA Kit	Thermo Fisher Scientific	Catalog# BMS610
Experimental Models: Cell Lines		
Mouse: B16F0 cells	ECACC	EC92101204
Mouse: B16F10 cells	ATCC	CRL-6475
Experimental Models: Organisms/Strains		
Mouse: C57BL/6	CLEA Japan	N/A
Mouse: C57BL/6	Charles River Laboratories	N/A
Mouse: B6.129S6-Rag2tm1Fwa N12	Taconic	Taconic: RAGN12
Mouse: B10;B6-Rag2tm1Fwa Il2rgtm1Wjl	Taconic	Taconic: 4111
Mouse: Il1rl1$^{-/-}$	Laboratory of Dr. K. Nakanishi	N/A
Oligonucleotides		
LDHA (Gene ID 16828) Mouse shRNA	OriGene	Catalog# TF515371
Software and Algorithms		
GraphPad Prism 6	GraphPad Software	https://www.graphpad.com
FlowJo 10 (version 10.0.7)	Tree Star	https://www.flowjo.com
NIS-Elements AR (version 4.11)	Nikon	https://www.nikon.com

LEAD CONTACT AND MATERIALS AVAILABILITY

Further information and requests for resources and reagents should be directed to and will be fulfilled by the Lead Contact, Shigeo Koyasu (shigeo.koyasu@riken.jp).

This study did not generate new unique reagents.

EXPERIMENTAL MODEL AND SUBJECT DETAILS

Mice

Eight-week-old male or retired female C57BL/6 mice were purchased from Charles River Laboratories, Japan or CLEA, Japan and maintained under specific pathogen-free conditions in the animal facility at the RIKEN Center for Integrative Medical Sciences, Yokohama, Japan. Retired female mice, defined as C57BL/6 mice older than four months of age and withdrawn from any further

breeding, were used for ILC2 isolation. *Rag2*$^{-/-}$ (stock no. RAGN12) and *Rag2*$^{-/-}$*Il2rg*$^{-/-}$ (stock no. 4111) mice were purchased from Taconic. *Il1rl1*$^{-/-}$ mice on a C57BL/6 background were a kind gift from Dr. K. Nakanishi of the Hyogo College of Medicine, Nishinomiya, Japan. Eight-to-twelve-week-old male mice were used for tumor growth studies. All animal experiments were approved by the Institutional Animal Care and Use Committees of the RIKEN and were performed in accordance with the institutional guidelines.

Cells and Complete Media

B16F0 (ECACC, EC92101204) and B16F10 (ATCC, CRL-6475) cells were grown at 37°C in 5% CO_2 in a humidified incubator in RPMI-1640 (Sigma Aldrich), supplemented with 10% FCS (Japan Bioserum), 100 μM nonessential amino acids (Sigma-Aldrich), 10 mM HEPES (Sigma-Aldrich), 1 mM sodium pyruvate (GIBCO), 100 U/ml penicillin (GIBCO), 100 μg/ml streptomycin (GIBCO), 50 μM 2-mercaptoethanol (GIBCO) and 400 μM L-glutamine (Lonza). Cells were detached with trypsin-EDTA (GIBCO) and passaged every 3 days.

ILC2s (Lin$^-$Sca1$^+$c-Kit$^+$ cells) were isolated from the mesentery as previously described (Moro et al., 2015) and cultured at 2,500 cells per well in 96-well round-bottom plates at 37°C in 5% CO_2 in a humidified incubator in RPMI-1640 (Sigma Aldrich), supplemented with 10% FCS (Japan Bioserum), 100 μM nonessential amino acids (Sigma-Aldrich), 10 mM HEPES (Sigma-Aldrich), 1 mM sodium pyruvate (GIBCO), 100 U/ml penicillin (GIBCO), 100 μg/ml streptomycin (GIBCO), 50 μM 2-mercaptoethanol (GIBCO) in the presence of 10 ng/ml mIL-2 (R&D Systems). The medium was replenished every other day.

B16F10 cells were transfected with the short hairpin RNA (shRNA) constructs cloned into the pGFP-V-RS plasmids to specifically knockdown expression of *Ldha* (Gene ID16828, OriGene). Untransfected cells (WT) and cells transfected with a non-specific, scrambled shRNA (CTRL) served as controls.

Human Samples

Commercially available formalin-fixed paraffin embedded (FFPE) human malignant melanoma tissue array was purchased from US Biomax, Inc (USA).

METHOD DETAILS

Tumor Cell Implantation

For tumor cell implantation, mice were anesthetized with 1% isoflurane in combination with O_2 and N_2. Tumor cells (1x10^6 cells per mouse) alone or admixed with ILC2s (1x10^5 cells per mouse) in 100 μL PBS were inoculated subcutaneously and dorsolaterally. For adipose tissue studies, tumor cells were inoculated into the anterior subcutaneous adipose tissue depot as previously described (Wagner et al., 2012). Tumor-associated adipose tissue was collected by microdissection under a stereoscopic microscope. Control adipose tissue from the counterpart depot was collected from age- and sex-matched animals. For IL-33 treatment, mice were administered IL-33 (0.5 μg in 100 μL PBS) or PBS alone intraperitoneally at the time of tumor implantation and every 3 days thereafter. For NK cell depletion, mice were administered anti-asialo GM1 (ASGM1) antibody (0.3 mg in 100 μL PBS) or control IgG (0.3 mg in 100 μL PBS) intraperitoneally the day before tumor implantation, at the time of tumor implantation and every 3 days thereafter. The depletion efficiency was verified by flow cytometric analysis using spleen NK cells. Anti-ASGM1-treated mice possessed 2.1% (±0.3%, s.e.m.) CD3$^-$NK1.1$^+$ NK cells compared with 11.5% (±1.4%, s.e.m.) in control IgG-treated mice. The mice were administered IL-33 or PBS as previously described. Tumor size was measured daily using a vernier caliper.

Conditioned Medium Preparation

Conditioned medium (CM) was prepared from B16F10 cells (6x10^6 cells) plated into three 25 cm^2 BD Falcon flasks (BD Biosciences). Samples of CM were collected on days 1, 2, 3 and 4, transferred to 15 mL BD Falcon tubes (BD Biosciences) and centrifuged at 1300 rpm for 10 minutes as described elsewhere (Colegio et al., 2014). Samples were then sterile-filtered (0.22 μm) (Millipore) and kept at −20°C for future experiments.

Hanging Drop Culture for Spheroid Formation and Co-Culture with ILC2s

B16F0 or B16F10 cells were plated as hanging drops on an inverted culture dish lid in 25 μL of complete medium at 10,000 cells/drop. The lid was then flipped and placed on a culture dish containing PBS to avoid evaporation. Hanging drop cultures were grown at 37°C up to 7 days in a humidified atmosphere with 5% CO_2. The medium was changed after 4 and 6 days of the culture period. The generation of spheroids in hanging drops was monitored using a stereomicroscope. B16F0 or B16F10 spheroids (3 spheroids/well) were then seeded in the bottom chamber, whereas ILC2s (25,000 cells/well) in the top chamber of a 6.5 mm (0.4 μm pore size) 24-well transwell (Corning) in complete RPMI-1640 medium in the presence of 10 ng/ml IL-2 (R&D Systems) and/or 10 ng/ml IL-33 (R&D Systems) for a period of 5 days. After 5 days of co-culture, ILC2s were collected and the number of viable cells counted in a haemocytometer using the Trypan Blue exclusion method. The same method was applied for the assessment of the survival of ILC2s cultured in CM or complete medium containing lactic acid, sodium lactate or HCl.

MTS Proliferation Assay

ILC2s were seeded into 96-well flat-bottom plates at a final density of 20,000 cells/well in 100 μL of medium supplemented with 10 ng/ml IL-2 (R&D Systems) and 10 ng/ml IL-33 (R&D Systems) with or without the presence of different concentrations of HCl, lactic acid (Sigma Aldrich) and sodium lactate (Sigma Aldrich) or in 100 μL of CM and its derivatives supplemented with 10 ng/ml IL-2 (R&D Systems) and 10 ng/ml IL-33 (R&D Systems). Unless stated otherwise, after 24 hours of incubation, each well was treated with 20 μL of a solution composed of 1.9 mg/ml of MTS [3-(4,5-dimethylthiazol-2-yl)-5-(3-carboxymethoxyphenyl)-2-(4-sulfophenyl)-2-tetrazolium, inner salt; MTS] in PBS (pH 6.0). The plate was then incubated for an additional 1 hour. The absorbance of the soluble formazan salt was measured against a tetrazolium standard, MTS solution.

Measurements of IL-5

IL-5 ELISA (Thermo Fisher Scientific) was performed as recommended by the manufacturer using supernatants of ILC2s seeded into 96-well round-bottom plates at a final density of 20,000 cells/well and cultured for 24 hours in 100 μL of medium supplemented with 10 ng/ml IL-2 (R&D Systems) and 10 ng/ml IL-33 (R&D Systems) with or without the presence of HCl, lactic acid (Sigma Aldrich) and sodium lactate (Sigma Aldrich) or in 100 μL of CM and its derivatives supplemented with 10 ng/ml IL-2 (R&D Systems) and 10 ng/ml IL-33 (R&D Systems).

Measurements of Lactic Acid

Cells were seeded into 96-well flat-bottom plates at a final density of 2,500 cells/well and cultured for 24 hours. Lactic acid concentration was measured in medium using L-Lactate Assay Kit (Abcam) and following the manufacturer's directions.

Giemsa Staining

Slides were coated with cell and tissue adhesive Cell-Tak (Corning) as recommended by the supplier. ILC2s cultured for 24 hours in 100 μL of medium supplemented with 10 ng/ml IL-2 (R&D Systems) alone or in combination with 10 ng/ml IL-33 (R&D Systems) accompanied with the presence of lactic acid (Sigma Aldrich), sodium lactate (Sigma Aldrich), HCl or in 100 μL of CM and its derivatives supplemented with 10 ng/ml IL-2 (R&D Systems) and 10 ng/ml IL-33 (R&D Systems) were transferred onto slides, washed, dried, fixed with methanol (Sigma Aldrich) and stained with Giemsa (Muto). The diameter of ILC2s was determined from 100 cells/group using NIS-elements AR software from Nikon.

Immunohistochemistry

Tumor or adipose tissue samples were collected and fixed in 4% paraformaldehyde, paraffin-embedded, and cut into 4 μm sections. For immunolabeling, paraffin-embedded tissue sections were dewaxed, rehydrated and boiled in a water bath at 98°C for 20-40 minutes in 10 mM citrate buffer (pH 6.0) or Tris/EDTA buffer (pH 9.0). Antigen retrieval for F4/80 staining was performed with Proteinase K (Dako) treatment following the manufacturer's instructions. The sections were then blocked with diluted serum from the secondary antibody host for 30 minutes, and incubated for 1 hour or overnight at 4°C with the primary antibody. Endogenous peroxidase activity was blocked for 30 minutes with 3% hydrogen peroxide (Sigma-Aldrich) and a biotinylated anti-rat, anti-rabbit or anti-goat secondary antibody (Vector Laboratories) was applied for 30 minutes. The antigen-antibody complex reaction was augmented with avidin-biotin-peroxidase for 30 minutes following the manufacturer's instructions (Vectastain Elite ABC HRP Reagent, Vector Laboratories) and incubated for 1-10 minutes with diaminobenzidine tetrahydrochloride (DAB, Dako). Next, sections were counterstained with hematoxylin (Thermo Fisher Scientific), dehydrated, and mounted with Entellan (Merck). The following antibodies were used for immunohistochemical analysis: rabbit anti-LYVE1 (1:250, catalog ab14917, Abcam), goat anti-CD31 (1:250, catalog sc1506, Santa Cruz Biotechnology), rabbit anti-Perilipin1 (1:250, catalog 9349, Cell Signaling), rat anti-CD3 (CD3-12) (1:100, catalog ab11089, Abcam), rabbit anti-CD8 (EPR21769) (1:1000, catalog ab217344, Abcam), rabbit anti-CD4 (EPR19514) (1:1000, catalog ab183685. Abcam), rabbit anti-CD11b (1:4000, catalog ab75476, Abcam), rat anti-F4/80 (CI:A3-1) (1:250, catalog ab6640, Abcam), rat anti-CD301 (ER-MP23) (1:100, catalog MCA2392, Bio-Rad), rabbit anti-MBP (AA100-215) (1:250, catalog ABIN1174871, Antibodies online), rabbit anti-IL-33 (1:250, catalog PAB980Mu01, Cloud-Clone Corp) and rabbit anti-IL-33 (1:50, catalog MAB36252, R&D Systems).

Picrosirius Red Staining

Paraffin-embedded sections were deparaffinized and rehydrated. The slides were then stained with picrosirius red solution composed of picric acid and Direct Red 80 (both Sigma-Aldrich) following the manufacturer's instructions and dehydrated. Tissue sections were then washed in 2 changes of acidified water after picrosirius red staining.

Flow Cytometry

Tumor samples were incubated in Collagenase D (1 mg/ml, Roche) for 1 hour at 37°C followed by 100 mM EDTA and then mechanically dissociated by passage through a 70 μm strainer to create a single-cell suspension. ILC2s were isolated from the mesenteric and inguinal subcutaneous adipose tissue as previously described (Moro et al., 2010, 2015). To isolate cutaneous ILC2s, 1.5 × 1.5 cm skin samples overlying tumors were incubated in Liberase TH (0.1 mg/ml, Roche) for 1 hour at 37°C then mechanically dissociated using gentleMACS (Miltenyi Biotec) and purified by density centrifugation with 30% Percoll (Sigma Aldrich). ILC2s from lymph nodes were passaged through a 70 μm strainer. Isolated cells were suspended in HBSS containing 2% FBS and 0.2% sodium azide.

The following anti-mouse antibodies were used for flow cytometry: CD3ε (145-2C11), CD4 (GK1.5), CD8α (53-6.7), CD11c (HL3), NK1.1 (PK136), CD19 (1D3), CD11b (M1/70), TER119 (TER119), Gr-1 (RB6-8C5), CD5 (53-7.3), Ly6A/E (Sca1) (D7 or E13-161.7), KLRG1 (2F1), CD45.2 (104), c-Kit (2B8), Thy1.2 (53-2.1), T1/ST2 (DJ8), CD25 (APC/Cy7), Siglec-F (E50-2440) and fluorochrome-conjugated streptavidin were purchased from BD Biosciences whereas antibodies against mouse FcεRIα (MAR-1) were from BioLegend. Antibodies against mouse CD16/CD32 (2.4G2) were purified from hybridoma culture supernatants in our laboratory. Cell viability was determined using propidium iodide. Cells were analyzed using FACSCalibur and sorted using FACSAria III. All data were analyzed using FlowJo software (TreeStar). The gating strategy is provided as supplemental information (Figure S1). A hemocytometer-based trypan blue dye exclusion cell quantitation was performed to estimate the total number of cells.

QUANTIFICATION AND STATISTICAL ANALYSIS

Database Analysis

The association between gene expression and survival rate of 458 melanoma patients was determined with recently described Oncolnc platform (www.oncolnc.org) using the publicly available TCGA (https://www.cancer.gov/about-nci/organization/ccg/research/structural-genomics/tcga) database (Anaya, 2016). According to the expression level of *IL33* or *SIGLEC8*, the 458 melanoma samples were assigned into two groups of low and high expression levels of *IL33* or *SIGLEC8*, each of them containing 229 samples. Expression data were extracted and the Kaplan–Meier estimation curve was plotted using Prism software (GraphPad Inc.).

The gene expression correlation analysis was performed on the ''Tumour Skin Cutaneous Melanoma - TCGA - 470 - rsem – tcgars'' dataset containing data from 470 melanoma patients from the publicly available TCGA (https://www.cancer.gov/about-nci/organization/ccg/research/structural-genomics/tcga) database using the microarray analysis and visualization platform R2 (https://hgserver1.amc.nl:443/). Pearson's correlation coefficient, r, was calculated with the transform 2log setting. Expression data of the genes of interest were extracted and represented using Prism software (GraphPad Inc.).

Statistics

Unless otherwise stated, results are representative of at least two independent experiments. Statistical significance was analyzed by the unpaired, two-tailed Student's t test or one-way ANOVA followed by Tukey's multiple comparisons test using Prism software (GraphPad Inc.). A p value less than 0.05 was considered to be statistically significant. p values less than 0.05, 0.01 or 0.001 were labeled with *, ** or ***, respectively. Data were expressed as average ± s.e.m. Whenever possible, the investigator was partially blinded for assessing the outcome (e.g., measurements in mouse studies and immunohistochemistry). To determine the correlation between gene expression levels in skin cutaneous melanoma patients in the TCGA dataset, Pearson's correlation coefficient, r, was calculated. To demonstrate the association between gene expression levels and survival rate of skin cutaneous melanoma patients in the TCGA dataset, multivariate Cox regression and Kaplan–Meier analysis were performed. Expression data of the genes of interest were extracted and the Kaplan–Meier estimation curve was plotted using Prism software (GraphPad Inc.).

DATA AND CODE AVAILABITY

This study did not generate any unique datasets or code.